The neutron number probability distribution in coupled lumped assemblies

O'Rourke, Patrick Francis
Prinja, Anil Kant

To be published in: Annals of Nuclear Energy

DOI to publisher's version: 10.1016/j.anucene.2023.110063

The Neutron Number Probability Distribution in Coupled Lumped Assemblies

Patrick F. O'Rourke*

XTD Applied Physics
Los Alamos National Laboratory
PO Box 1663, MS T082
Los Alamos, NM 87545, USA

Anil K. Prinja

Department of Nuclear Engineering
University of New Mexico
Albuquerque, NM 87131, USA

Abstract

The validity of the gamma distribution in describing the neutron number probability distribution function for both isolated and coupled multiplying assemblies when constrained to reproduce the true mean and variance is investigated in lumped geometry by numerical comparison with kinetic Monte Carlo simulations. The mean and variance are obtained from numerical solution of moment equations constructed from the relevant forward Master equation with assembly coupling coefficients obtained from a view factor method. Numerical results for a two-group, two coupled assemblies model, with static and dynamic reactivity insertion, show that that except for subcritical assemblies, the gamma distribution well-approximates the number distribution. Differences in the fast and thermal neutron population shapes are explained in terms of effective source strengths due to downscatter and coupling.

Keywords: Stochastic population, Master equation, coupled point assemblies, gamma distribution
2010 MSC: 00-01, 99-00

1. Introduction

Large and persistent random fluctuations in the neutron number is a characteristic feature of neutron populations in fissile assemblies containing weak intrinsic random sources such as spontaneous fission. The emergence of deterministic behavior is prevented by the weak overlap of neutron chains spawned by the internal sources. In general, low order statistical moments like the mean and variance of the neutron density, when considered in isolation, cannot adequately describe the instantaneous state of the neutron population. Probabilistic quantities such as the chain survival and divergence probabilities and in particular the probability distribution function (pdf) of the number of neutrons are more relevant measures of strongly stochastic neutron populations, all of which can in principle be obtained from appropriately formulated forward or backward Master equations [1, 2, 3]. Although these formulations yield explicit, closed equations for the survival and divergence probabilities, which have been solved numerically under quite general conditions [4, 5, 6], it is not practical to solve the Master equations directly for the neutron number pdf. Monte Carlo simulation has thus far been the only practical, if laborious, computational approach to obtaining neutron distributions. However, insightful analytical solutions have been obtained in lumped (point kinetic) geometry by introducing physically reasonable approximations. For instance, Bell [1] obtained closed form solutions to the forward Master equation (FME) for the time dependent neutron pdf in supercritical assemblies, showing that in the absence of delayed neutrons and at late times, the neutron

*Corresponding author

pdf is well-approximated by the gamma distribution. In particular, the distribution highlights the transition of the neutron population from a stochastic to a deterministic regime with increasing source strength [7, 8].

Although Bell derived the gamma distribution by solving the FME, in the process delineating the strict conditions for its validity, this distribution had earlier been heuristically posited as the simplest two-parameter continuous pdf with semi-infinite support (i.e., non-Gaussian) to describe stochastic neutron populations. The parameters were uniquely determined by relating them to quantities that could be independently and accurately determined. Harris [9] showed that fixing the parameters so that the distribution reproduced the correct mean and variance of the neutron number, which were assumed to be independently and exactly obtained from the mathematically simpler moment equations, the gamma distribution was in fact more broadly applicable in describing stochastic neutron phenomena than the strict conditions of Bell's derivation would lead one to expect. For instance, when time dependent (linear-ramp) reactivity excursions and delayed neutrons are incorporated, the gamma distribution quantitatively predicts the preinitiation probability of fast burst reactors as well as the time to transition to a deterministic phase in these systems [9, 10, 11]. More interestingly, when compared against benchmark Monte Carlo simulations in a preliminary study [12], the gamma distribution with exact mean and variance has been shown to approximate the distribution of the total number of neutrons in a finite assembly surprisingly well even when the neutron phase space dependence is retained. One is led to speculate that the gamma distribution is a universally valid, although inexact, pdf for the total neutron number in an increasing population, i.e., in regimes where population extinction is improbable, when second-order statistics dominate the stochasticity of the population.

The objective of the present work is to (i) assess the validity of the Harris ansatz under varying neutron multiplication conditions in lumped geometry, by comparing the distribution to simulation results obtained using Gillespie's [13] kinetic Monte Carlo method, and (ii) investigate the applicability of the Harris ansatz to coupled lumped fissile assemblies in one and two neutron energy groups. A forward Master equation for the single-time joint distribution of neutron number in each assembly, accounting for transfer of neutrons from one assembly to another via leakage, is introduced from which equations for low-order statistical moments are developed. Besides the mean and variance, it is necessary to additionally compute the correlation function between the assemblies because of the neutronic coupling. Both static and dynamic reactivity conditions are considered, although a formal mechanism that is responsible for reactivity coupling between assemblies is not considered or proposed. Following Harris, it is then hypothesized that the number distribution in each assembly is a gamma distribution, with assembly-specific means and variances obtained by numerically solving the coupled moment equations. The gamma distribution for each assembly is then compared against distributions obtained by Monte Carlo simulation. The assembly coupling probabilities are computed using a previously developed view factor method [14].

The forward Master equation and its moment equations are presented in Sec. 2, along with a discussion of the Harris ansatz. We then describe the Stochastic Simulation Algorithm (SSA), a state-space kinetic Monte Carlo method, in Sec. 3. A discussion of the calculation of the point kinetics parameters that provide data for the SSA and moments computation is presented in Section 4 followed by a brief discussion on the numerical solution of the moment equations in Section 5. Extensive numerical results are then presented in Section 6 covering the following configurations: subcritical and supercritical assemblies, one-group fast neutrons and two-group fast and thermal neutrons, as well as static and dynamic reactivity. We close with some concluding remarks in Sec. 7.

2. Forward Master Equation and Moment Equations

We consider a system of J coupled multiplying assemblies and express the stochastic state of the system by $\mathbf{n} = \{n_{g,j},\, j = 1, 2, \ldots J,\, g = 1, 2\}$, the components of which represent the fast ($g = 1$) and thermal ($g = 2$) neutron numbers in the individual assemblies. We are interested in $P_{\mathbf{n}}(t)$, the joint probability that at time t there exist $n_{1,1}$ fast neutrons and $n_{2,1}$ thermal neutrons in assembly-1, and so on for assemblies $2, 3, \ldots, J$. The state of the system, and hence the probability of finding the system in a particular state, changes with time as a result of mutually exclusive events or collisions with known transition probabilities. Let $\lambda^j_{c,g}\ \mathrm{d}t$, $\lambda^j_{f,g}\ \mathrm{d}t$, $\lambda^j_{\ell,g}\ \mathrm{d}t$, and $\lambda^j_{s,g\to g'}\ \mathrm{d}t$ be the single neutron transition probabilities for capture, fission, leakage, and

scattering or group transfer, in incremental time $\mathrm{d}t$ in assembly-j and energy group-g. The probability per unit time for any collision event to occur is then

$$\lambda_{t,g}^{j} = \lambda_{f,g}^{j} + \lambda_{c,g}^{j} + \lambda_{\ell,g}^{j} + \sum_{g' \neq g} \lambda_{s,g\to g'}^{j}, \tag{1}$$

where within group scattering ($\lambda_{s,g\to g}^{j}$) is excluded as it does not alter the system state. The prompt fission neutron multiplicity distribution is given by $q_{\nu,g}^{f,j}, \nu = 1, 2, \ldots, \nu_{m,g}^{f,j}$, which is the probability that ν neutrons are emitted in a fission event in assembly-j and $\nu_{m,g}^{f,j}$ is the maximum possible number of neutrons that may be emitted in a fission event that is induced by a neutron in energy group g. Delayed neutrons are neglected in this investigation but can be readily incorporated by expanding the state space to accommodate an arbitrary number of precursor nuclei. $S_g^j(t)\,\mathrm{d}t$ is the probability of a source event in a short time interval $\mathrm{d}t$ in assembly-j producing neutrons in group g, with associated multiplicity distribution $q_{\nu,g}^{S,j}, \nu = 1, 2, \ldots, \nu_{m,g}^{S,j}$. Finally, upon leaking from assembly j, the probability of a neutron then streaming and entering assembly k is defined as $p_{j\to k}$, $j \neq k = 1, 2, \ldots, J$ and the probability that a leaked neutron does not intercept another assembly is given by $p_{j\to\infty}$, with the normalization $\sum_{k\neq j}^{J} p_{j\to k} + p_{j\to\infty} = 1$.

Further assuming that only thermal neutrons induce fission, only fast neutrons are born in both induced fission and spontaneous fission events, and there is no upscatter from the thermal to the fast group, the standard last-step probability balance arguments applied to all mutually exclusive and independent events yields the forward Master equation[1, 3] :

$$\frac{\mathrm{d}P_{\mathbf{n}}(t)}{\mathrm{d}t} + \sum_{j=1}^{J}\left\{ S_1^j + \sum_{g=1}^{2} n_{g,j}\lambda_{t,g}^{j} \right\} P_{\mathbf{n}}(t) = \sum_{j=1}^{J}\Bigg\{ (n_{1,j}+1)\lambda_{s,1\to 2}^{j} P_{\mathbf{n}+\boldsymbol{\delta}_{1,j}-\boldsymbol{\delta}_{2,j}}(t) \tag{2}$$

$$+ S_1^j \sum_{\nu=0}^{\nu_{m,1}^{S,j}} q_{\nu,1}^{S,j} P_{\mathbf{n}-\nu\boldsymbol{\delta}_{1,j}}(t) + (n_{2,j}+1)\lambda_{f,2}^{j} \sum_{\nu=0}^{\nu_{m,2}^{f,j}} q_{\nu,2}^{f,j} P_{\mathbf{n}+\boldsymbol{\delta}_{2,j}-\nu\boldsymbol{\delta}_{1,j}}(t) \tag{3}$$

$$+ \sum_{g=1}^{2}(n_{g,j}+1)\left[\lambda_{c,g}^{j} P_{\mathbf{n}+\boldsymbol{\delta}_{g,j}}(t) + \lambda_{\ell,g}^{j}\left(p_{j\to\infty} P_{\mathbf{n}+\boldsymbol{\delta}_{g,j}}(t) + \sum_{\substack{k=1\\k\neq j}}^{J} p_{j\to k} P_{\mathbf{n}+\boldsymbol{\delta}_{g,j}-\boldsymbol{\delta}_{g,k}}(t) \right) \right] \Bigg\} \tag{4}$$

with the initial condition

$$P_{\mathbf{n}}(t=0) = \prod_{j=1}^{J}\prod_{g=1}^{2} \delta_{n_{g,j},N_{g,j}}, \tag{5}$$

where $\delta_{i,j}$ is the Kronecker delta function and $N_{g,j}$ is the initial population of neutrons in energy group g and assembly j. We have defined $\boldsymbol{\delta}_{g,j}$ as a unit vector with (g,j) the only nonzero element.

Equations for the moments of this joint distribution are more conveniently constructed by first expressing the forward Master equation in terms of the probability generating function (PGF), which is defined as:

$$G(\mathbf{x},t) = \sum_{j=1}^{J}\sum_{g=1}^{2}\sum_{n_{g,j}=0}^{\infty}\prod_{j'=1}^{J}\prod_{g'=1}^{2} x_{g',j'}^{n_{g',j'}} P_{\mathbf{n}}(t), \tag{6}$$

where $x_{g,j} \in [0,1]$, is the transform variable for the neutron number in group g and assembly-j and we define $\mathbf{x} = \{x_{g,j},\, j = 1, 2, \ldots, J,\, g = 1, 2\}$. Multiplying Eq. 2 by the product of $x_{g',j'}^{n_{g',j'}}$ for all g', j' and summing over all g, j, and corresponding $n_{g,j}$, we obtain after some algebraic manipulation the following partial differential equation for the PGF:

$$\frac{\partial G(\mathbf{x},t)}{\partial t} = \sum_{j=1}^{J}\Bigg[S_1^j\Big[h_{S,1}^{j}(x_{1,j}) - 1\Big] G(\mathbf{x},t) + \lambda_{s,1\to 2}^{j} x_{2,j}\frac{\partial G}{\partial x_{1,j}} + \lambda_{f,2}^{j} h_{f,2}^{j}(x_{1,j})\frac{\partial G}{\partial x_{2,j}} \tag{7}$$

$$+ \sum_{g=1}^{2}\left(-\lambda_{t,g}^{j} x_{g,j} + \lambda_{c,g}^{j} + \lambda_{\ell,g}^{j}\left\{ p_{j\to\infty} + \sum_{\substack{k=1\\k\neq j}}^{J} p_{j\to k} x_{g,k} \right\} \right)\frac{\partial G}{\partial x_{g,j}} \Bigg] \tag{8}$$

with the initial condition

$$G(\mathbf{x},0)=\prod_{j=1}^{J}\prod_{g=1}^{2}x_{g,j}^{N_{g,j}}. \tag{9}$$

Here, the generating function for the multiplicity distribution for fission process ζ, induced or spontaneous, is defined as:

$$h_{\zeta,g}^{j}(x_{i,k})=\sum_{\nu=0}^{\nu_{m}^{\zeta,j}}q_{\nu,g}^{\zeta,j}\cdot x_{i,k}^{\nu}, \tag{10}$$

with the normalization $h_{\zeta,g}^{j}(x_{i,k}=1)=1$.

2.1. Moment Equations for Two Coupled Assemblies

We now derive equations for the moments of the neutron number pdf for the mean, variance, and correlations strictly for a system composed of two coupled assemblies, thus we restrict $J=2$. Equations for the moments may be obtained by taking successive derivatives of G with respect to components of $\mathbf{x}$ and evaluating at $\mathbf{x}=\mathbf{1}$. The first few moments that are pertinent to the ensuing study are:

$$\overline{n}_{g,j}(t)=\left.\frac{\partial G(\mathbf{x},t)}{\partial x_{g,j}}\right|_{\mathbf{x}=\mathbf{1}} \tag{11a}$$

$$\overline{n_{g,j}(n_{g,j}-1)}(t)=\overline{n_{g,j}^{2}}-\overline{n}_{g,j}(t)=\left.\frac{\partial^{2}G(\mathbf{x},t)}{\partial x_{g,j}^{2}}\right|_{\mathbf{x}=\mathbf{1}} \tag{11b}$$

$$\overline{n_{1,j}n_{2,j}}(t)=\left.\frac{\partial^{2}G(\mathbf{x},t)}{\partial x_{1,j}\,\partial x_{2,j}}\right|_{\mathbf{x}=\mathbf{1}}, \tag{11c}$$

where Eq. 11a defines the average of the neutron population in energy group g and assembly-j, Eq. 11b defines the average of the second factorial moment of the population of energy group g and assembly-j, and Eq. 11c defines the correlation between the fast and thermal population in assembly-j. Using similar identities, other moments may be obtained by mixing the necessary derivatives. By applying the identity given by Eq. 11a to the PGF PDE, Eq. 7, we obtain a system of coupled linear ODEs for the fast and thermal moments in assembly-j:

$$\frac{\mathrm{d}\overline{n}_{1,j}(t)}{\mathrm{d}t}=-\lambda_{t,1}^{j}\overline{n}_{1,j}(t)+\overline{\nu}_{f,2}^{j}\lambda_{f,2}^{j}\overline{n}_{2,j}(t)+\overline{\nu}_{S,1}^{j}S_{1}^{j}+\sum_{\substack{k=1\\k\neq j}}^{J}\lambda_{\ell,1}^{k}p_{k\to j}\overline{n}_{1,k}(t) \tag{12a}$$

$$\frac{\mathrm{d}\overline{n}_{2,j}(t)}{\mathrm{d}t}=-\lambda_{t,2}^{j}\overline{n}_{2,j}(t)+\lambda_{s,_{1\to2}}^{j}\overline{n}_{1,j}(t)+\sum_{\substack{k=1\\k\neq j}}^{J}\lambda_{\ell,2}^{k}p_{k\to j}\overline{n}_{2,k}(t), \tag{12b}$$

with the initial conditions given by $\overline{n}_{g,j}(0)=N_{g,j}$. We have also defined the average number of neutrons emitted in the fission process ζ to be

$$\overline{\nu}_{\zeta,g}^{j}=\left.\frac{\mathrm{d}h_{\zeta,g}^{j}(x_{i,k})}{\mathrm{d}x_{_{i,k}}}\right|_{x_{_{i,k}}=1} \tag{13}$$

where $\overline{\nu}_{f,2}^{j}$ in this model is explicitly the average number of fast neutrons emitted due to a thermal neutron induced fission and $\overline{\nu}_{S,1}^{j}$ is the average number of fast neutrons emitted in a source decay event.

Using the Pochhammer shorthand notation for the falling factorial,

$$(\nu)_{k}=\nu(\nu-1)(\nu-2)\cdots(\nu-k+1)=\prod_{i=0}^{k-1}(\nu-i),\qquad k=1,2,\ldots, \tag{14}$$

equations for the second moments of the fast and thermal population in assembly-j are:

$$\frac{\mathrm{d}\overline{n_{1,j}^2}(t)}{\mathrm{d}t} + 2\lambda_{t,1}^j \overline{n_{1,j}^2}(t) = \frac{\mathrm{d}\overline{n}_{1,j}}{\mathrm{d}t} + 2\left(\lambda_{t,1}^j + \overline{\nu}_{S,1}^j S_1^j\right)\overline{n}_{1,j}(t) + 2\overline{\nu}_{f,2}^j \lambda_{f,2}^j \overline{n_{1,j} n_{2,j}}(t) + \overline{(\nu_{f,2}^j)_2} \lambda_{f,2}^j \overline{n}_{2,j}(t) + \overline{(\nu_{S,1}^j)_2} S_1^j + 2\sum_{\substack{k=1 \\ k\neq j}}^{J} \lambda_{\ell,1}^k p_{k\to j} \overline{n_{1,j} n_{1,k}}(t) \tag{15a}$$

$$\frac{\mathrm{d}\overline{n_{2,j}^2}(t)}{\mathrm{d}t} + 2\lambda_{t,2}^j \overline{n_{2,j}^2}(t) = \frac{\mathrm{d}\overline{n}_{2,j}}{\mathrm{d}t} + 2\lambda_{t,2}^j \overline{n}_{2,j}(t) + 2\lambda_{s,1\to 2}^j \overline{n_{1,j} n_{2,j}}(t) + 2\sum_{\substack{k=1 \\ k\neq j}}^{J} \lambda_{\ell,2}^k p_{k\to j} \overline{n_{2,j} n_{2,k}}(t) \tag{15b}$$

for which the initial conditions are $\overline{n_{g,j}^2}(0) = N_{g,j}^2$. We also require equations for the correlated moments, which may be similarly obtained as:

$$\frac{\mathrm{d}\overline{n_{1,j} n_{2,j}}}{\mathrm{d}t} + (\lambda_{t,1}^j + \lambda_{t,2}^j)\overline{n_{1,j} n_{2,j}} = \lambda_{s,1\to 2}^j \left(\overline{n_{1,j}^2} - \overline{n}_{1,j}\right) + \overline{\nu}\lambda_{f,2}^j \left(\overline{n_{2,j}^2} - \overline{n}_{2,j}\right) + \overline{\nu} S_1^j \overline{n}_{2,j} + \sum_{\substack{k=1 \\ k\neq j}}^{2} p_{k\to j}\left(\lambda_{\ell,1}^k \overline{n_{1,k} n_{2,j}} + \lambda_{\ell,2}^k \overline{n_{1,j} n_{2,k}}\right) \tag{16a}$$

$$\frac{\mathrm{d}\overline{n_{1,1} n_{1,2}}}{\mathrm{d}t} + (\lambda_{t,1}^1 + \lambda_{t,1}^2)\overline{n_{1,1} n_{1,2}} = \overline{\nu}\lambda_{f,2}^1 \overline{n_{1,2} n_{2,1}} + \overline{\nu}\lambda_{f,2}^2 \overline{n_{1,1} n_{2,2}} + \overline{\nu} S_1^1 \overline{n}_{1,2} + \overline{\nu} S_1^2 \overline{n}_{1,1} + \lambda_{\ell,1}^1 p_{1\to 2}\left(\overline{n_{1,1}^2} - \overline{n}_{1,1}\right) + \lambda_{\ell,1}^2 p_{2\to 1}\left(\overline{n_{1,2}^2} - \overline{n}_{1,2}\right) \tag{16b}$$

$$\frac{\mathrm{d}\overline{n_{2,1} n_{2,2}}}{\mathrm{d}t} + (\lambda_{t,2}^1 + \lambda_{t,2}^2)\overline{n_{2,1} n_{2,2}} = \lambda_{s,1\to 2}^1 \overline{n_{1,1} n_{2,2}} + \lambda_{s,1\to 2}^2 \overline{n_{1,2} n_{2,1}} + \lambda_{\ell,2}^1 p_{1\to 2}\left(\overline{n_{2,1}^2} - \overline{n}_{2,1}\right) + \lambda_{\ell,2}^2 p_{2\to 1}\left(\overline{n_{2,2}^2} - \overline{n}_{2,2}\right) \tag{16c}$$

$$\frac{\mathrm{d}\overline{n_{g,1} n_{h,2}}}{\mathrm{d}t} + (\lambda_{t,g}^1 + \lambda_{t,h}^2)\overline{n_{g,1} n_{h,2}} = \overline{\nu}\lambda_{f,2}^g \overline{n_{2,1} n_{2,2}} + \overline{\nu} S_1^g \overline{n}_{2,h} + \lambda_{s,1\to 2}^h \overline{n_{1,1} n_{1,2}} + \lambda_{\ell,h}^1 p_{1\to 2} \overline{n_{1,1} n_{2,1}} + \lambda_{\ell,g}^2 p_{2\to 1} \overline{n_{1,2} n_{2,2}} \tag{16d}$$

where it is understood that $\overline{\nu} S_g^j = \overline{\nu}_{S,g}^j S_g^j$, and $\overline{\nu}\lambda_{f,g}^j = \overline{\nu}_{f,g}^j \lambda_{f,g}^j$ and the initial conditions are simply the products of the respective initial populations of the solutions (e.g., $\overline{n_{g,j} n_{g',j'}}(0) = N_{g,j} N_{g',j'}$). For the case of 2 coupled assemblies, we will need to solve a system of 14 ODEs in order to determine the means and variances of the 4 respective neutron number pdfs. First, however, we provide some background discussion in the next section on the role of the gamma distribution in characterizing the stochastic development of the neutron population.

2.2. The Gamma Distribution

As discussed earlier, the objective of this article is to assess the validity of heuristically characterizing the stochastic neutron population in coupled assemblies with a gamma distribution. However, it should be remarked that the choice of the gamma distribution for this purpose is neither arbitrary nor fortuitous but in fact has a rigorous foundation. As first demonstrated by Bell [1], the gamma distribution is the time-asymptotic solution of the single assembly, one-group FME in a supercritical assembly when the mean

neutron population is sufficiently large. It is instructive to briefly review Bell's solution here to provide perspective and motivate the ensuing work.

Specializing to a single assembly and single energy neutrons and defining the associated generating function as $G(x,t) = \sum_{n=0}^{\infty} x^n P_n(t)$, Eq. 7 reduces to

$$\frac{\partial G(x,t)}{\partial t} = S(x-1)G(x,t) + \left[\lambda_f h_f(x) - \lambda_t x + \lambda_c\right]\frac{\partial G(x,t)}{\partial x}, \tag{17}$$

with

$$G(x,0) = 1, \tag{18}$$

corresponding to no neutrons present in the system prior to the initial time. Equation 17, in which leakage has been subsumed into capture and a singlet emitting source is assumed, is identical to the generating function equation considered by Bell [1]. This equation can be formally solved by the method of characteristics but does not yield a closed form solution for a general fission multiplicity generating function $h_f(x)$. However, an approximate closed-form solution for $G(x,t)$ valid for $x \sim 1$ can be developed by expanding $h_f(x)$ in powers of $1 - x \ll 1$, and neglecting third and higher order terms [1]. When inverted, this solution gives the large n approximation to $P_n(t)$. In this so-called quadratic approximation, the generating function equation is readily solved assuming a constant source strength to give the solution [1, 8]

$$G(x,t) = \left[1 - \frac{\overline{n}(t)}{\eta}(x-1)\right]^{-\eta}, \tag{19}$$

where $\overline{n}(t)$ is the mean neutron number, which is exact in this approximation and arises in explicit form in the solution but, relevant to this work, can also be obtained from the first moment equation. The parameter η is related to the source strength through

$$\eta = \frac{2\,S}{\lambda_f\,\overline{\nu(\nu-1)}}, \tag{20}$$

where $\overline{\nu(\nu-1)}$ is the second factorial moment of the fission neutron multiplicity distribution. We emphasize that the assembly has been assumed to be supercritical with the condition $\overline{n}(t) \gg 1$. The generating function in Eq. 19 can be readily inverted to yield for the neutron number distribution [1, 8]

$$P(n,t) = \left(\frac{\eta}{\overline{n}(t)}\right)^{\eta} \frac{n^{\eta-1}}{\Gamma(\eta)} \exp\left(-\frac{n\eta}{\overline{n}(t)}\right), \quad 0 < n < \infty, \tag{21}$$

where n is now a continuous variable. Equation 21 is a gamma distribution $\Gamma(n|\eta, \eta/\overline{n}(t))$ with shape parameter η and inverse scale parameter $\eta/\overline{n}(t)$, normalized to unity over $(0, \infty)$. The gamma distribution in Eq. 21 may be expressed in self-similar form by setting $y = n/\overline{n}(t)$ to get

$$P(y,t) = \eta^{\eta}\,\frac{y^{\eta-1}}{\Gamma(\eta)} \exp\left(-y\eta\right), \quad 0 < y < \infty. \tag{22}$$

The parameter η plays a unique role in characterizing the stochastic state of the neutron population at any given time, with the distribution qualitatively changing shape at $\eta = 1$ [8, 15]. The gamma distribution in Eq. 22 is monotonic for $\eta < 1$, giving a higher probability of finding neutron numbers less than the mean but with a tail that indicates neutron numbers much larger than the mean can exist. The range $\eta < 1$ therefore corresponds to one of stochastic volatility in the neutron population. In contrast, the distribution is unimodal for $\eta > 1$ and becomes increasingly peaked and centered around the mean neutron number $\overline{n}(t)$ as η increases beyond unity. The distribution was previously [8] shown to asymptotically approach a Gaussian and collapse to a delta function at the mean as $\eta \to \infty$. Thus $\eta = 1$ is a critical point that distinguishes a domain of strong stochasticity ($\eta < 1$) from one where the fluctuations diminish in strength ($\eta > 1$) and deterministic behavior begins to emerges. It can further be shown that to a good approximation $\eta \approx S\,\tau$ where $\tau = 1/\lambda_t$ is the neutron lifetime [8]. It follows that η is a measure of the number of source neutrons injected in one neutron

lifetime, immediately linking the stochastic state of the neutron population to the source strength. The above interpretation of the role of η will be helpful in understanding the numerical results of this investigation.

It is evident that the gamma distribution arises naturally in the characterization of neutron fluctuations in multiplying media with random intrinsic sources. Although explicitly derived for a particular set of approximations (growing mean neutron population, static conditions) it can be argued that the gamma distribution is not uniquely restricted by these approximations. That is, one can speculate that the distribution would be representative of the neutron population under more general conditions if the shape parameter η is taken to be dynamic and independently assigned. Indeed this has been demonstrated to be the case. Specifically, by selecting η such that the distribution also reproduces the exact variance of the neutron population under general conditions (dynamic reactivity, arbitrary source distribution) the transition of neutron population from a stochastic to deterministic state observed in fast burst reactors can be successfully described [9, 10, 11]. Moreover, there is some evidence that this ansatz, originally due to Harris [9], holds even when the neutron phase dependence (position, energy, direction) is retained [12]. In this case, the moment equations are the well known adjoint neutron transport equations [16]. Thus, as the mean and variance can be obtained from the mathematically much simpler, exact and numerically easily solved moment equations, it would appear that the highly complex problem of determining the probability distribution of the number of neutrons in a supercritical multiplying assembly as a function of time is reduced to the significantly simpler deterministic problem of solving a coupled set of linear moment equations.

The validity of the Harris ansatz is assessed in this work by comparing the gamma distribution against the true distribution obtained by Monte Carlo simulation. We further hypothesize and similarly verify that the gamma distribution remains valid for coupled assemblies where, in addition to preserving the consistent mean and variance of the true joint distribution, assembly coupling to a higher order is accounted for by also correctly preserving the first order correlation function. Proceeding by defining Eq. 21 for each assembly and obtaining the self-consistent η by equating the second moment of the gamma distribution to that given by the solution to the moment equations, we can write:

$$P^{(j)}(n,t) = \left(\frac{\eta_j(t)}{\overline{n}_j(t)}\right)^{\eta_j(t)} \frac{n^{\eta_j(t)-1}}{\Gamma(\eta_j(t))} \exp\left(-\frac{n\eta_j(t)}{\overline{n}_j(t)}\right), \qquad j = 1, 2, \ldots, J, \tag{23}$$

where $\eta_m(t)$ is defined by equating the variance obtained from Eq. 23 to the true variance obtained by solving the moment equations, giving

$$\eta_j(t) = \frac{\overline{n}_j^2(t)}{\overline{n_j^2}(t) - \overline{n}_j^2(t)} = \frac{\overline{n}_j^2(t)}{V_j(t)}. \tag{24}$$

To emphasize, this representation of the gamma distributions allows general induced and source fission multiplicity distributions and time varying assembly properties as well as a multigroup neutron energy structure to be incorporated with consistent second order statistics. We note that from the definition in Eq. 24, η_j is related to the relative standard deviation as

$$\frac{\sqrt{V_j(t)}}{\overline{n}_j(t)} = \frac{1}{\sqrt{\eta_j(t)}}, \tag{25}$$

which shows that the gamma distribution dynamically describes the variation from strongly stochastic to strongly deterministic through just the relative standard deviation of the population.

3. The Stochastic Simulation Algorithm

The Stochastic Simulation Algorithm (SSA) is a time dependent or kinetic Monte Carlo method developed by Gillespie for the study of the dynamics of chemical reactions [13], although the fundamentals had been known since the 1940s and 1950s with work done by Bartlett [17]. Applied to neutron populations, the SSA method samples time intervals between neutron collisions and the population state is updated based on

Table 1: Effects and associated probabilities for events considered.

Event, $e_{i,g,j}$	Prob($e_{i,g,j}$), $[s^{-1}]$	Effect		
		$n_{g,j}$	$n_{g,k}$	$n_{g',j}$
Source Emission	$S_g^j q_{\nu,g}^{S_j}$	$+\nu$		
Scatter	$n_{g,j}\lambda_{s,g\to g'}^j$	-1		+1
Capture	$n_{g,j}\lambda_{c,g}^j$	-1		
Induced Fission	$n_{g,j}\lambda_{f,g}^j q_{\nu,g}^{f,j}$	+(ν-1)		
Leakage & no Transfer	$n_{g,j}\lambda_{\ell,g}^j p_{j\to\infty}$	-1		
Leakage & Transfer from $j \to k$	$n_{g,j}\lambda_{\ell,g}^j p_{j\to k}$	-1	+1	

the different neutron reaction rates. The sum of the reaction rates is the state transition rate cumulative distribution function (CDF), which is simply obtained from the coefficients of the forward Master equation. In that sense, the SSA is effectively a direct simulation of the forward Master equation [18]. In general, one can solve the forward Master equation for arbitrary numbers of cells and energy groups [19, 20, 21, 22]. Additionally, previous work applied a version of SSA (referred to as the "discrete events dynamic system" simulation) to simulate the burst wait time pdf of several reactors [23].

In traditional event-based MC simulations, one simulates a single particle and samples distance and time intervals dependent on the cross-sections of the system the neutron is traversing. In the event of secondary particle production, one must save location and time of birth, and simulate those particles as well. In the SSA approach, we instead propagate the population state of the system and sample time intervals between events that transition the system to a new population state. The appeal of the SSA is that we do not need to allocate computer memory for all secondary particles and the associated phase-space coordinates but, rather, simply update the state of the system based off of those particles produced. In this section, we describe the implementation of the SSA algorithm to calculate the neutron number pdf in coupled assemblies.

Again, we consider J coupled assemblies with fast ($g = 1$) and thermal ($g = 2$) neutron populations $n_{g,j}$ and simulate the evolution of the neutron number in each assembly from initial time $t = 0$ to a final time t_f. Consistent with the arguments leading to the forward Master equation described in Sec. 2, we assume: an exclusively fast neutron source S_1^j in any assembly; fast neutron down-scatter to the thermal energy group with no up-scatter of thermal neutrons to the fast energy group; only thermal neutron induced fission which produces only fast neutrons; capture; leakage, and, upon leaking, potentially transferring to another assembly. Each of these events will alter the neutron population of the system with some associated probability and a particular following effect. We define the probability per unit time for the i^{th} event that fundamentally alters the population of neutrons in group g and assembly-j as $e_{i,g,j}$. Table 1 gives the different events with their associated probabilities and the resultant change in the neutron population.

We now discuss the SSA from a general point of view, and then reduce the scope to the algorithm we used for the results presented later. We define the state transition probability, $\mu(\mathbf{n}, t)$, as the probability per unit time that some event will occur at time t that will cause a departure from state $\mathbf{n}$, where $\mathbf{n} = \{n_{g,j},\, j = 1, 2, \ldots J,\, g = 1, 2\}$ is the stochastic state of the system. The transition probability is simply the sum of the individual event probability rates:

$$\mu(\mathbf{n}, t) = \sum_{j=1}^{J} \sum_{g=1}^{2} \sum_{i} \text{Prob}(e_{i,g,j}),$$

which from Table 1 can be expressed explicitly as

$$\mu(\mathbf{n}, t) = \sum_{j=1}^{J} \left\{ S_1^j + \sum_{g=1}^{2} n_{g,j}\lambda_{t,g}^j \right\}, \tag{26}$$

where the total state transfer rate for energy group g and assembly j is defined by Eq. 1. The rates are initially taken to be time independent, for purposes of demonstrating implementation of the algorithm in

static assemblies, but generalization to time dependent rates will be considered in Sec. 6.4. We emphasize that the rates are an input into the SSA and therefore assumed known. The algorithm then proceeds as follows:

1. Form a list of all rates in the system, i.e., calculate $\lambda^j_{\zeta,g}$ and S^j_g, where $\zeta = \{s, c, f, \ell\}$.
2. Initialize the system at time $t = 0$ with a predetermined initial neutron population state, $(\mathbf{n}, 0)$.
3. Calculate the cumulative function, $\mu(\mathbf{n}, t)$.
4. Obtain a uniform random number $\xi \in [0, 1]$.
5. Determine the event to carry out, i, in assembly j and energy group g by finding the indicies $\{i, g, j\}$ for which
$$\sum_{i',g',j'}^{i-1,g,j} \text{Prob}(e_{i',g',j'}) \;\leq\; \xi\mu \;<\; \sum_{i',g',j'}^{i,g,j} \text{Prob}(e_{i',g',j'})$$
Carry out event i and determine new population state, $\mathbf{n}'$.
6. Obtain another uniform random number $\xi \in [0, 1]$
7. Update the time with
$$t' \;=\; t \;+\; \Delta t$$
where $\Delta t \;=\; -\frac{1}{\mu}\ln(\xi)$
8. Update new state: $(\mathbf{n}, t) \rightarrow (\mathbf{n}', t')$
9. Either go to step 3 if $t' < t_f$ or terminate the simulation if $t' \geq t_f$.

Note that as the population and/or source strength increases, so does μ, causing the time intervals between events to decrease. If the population becomes too large, the sampled Δt may become unmanageably small and a lower bound on the time step must be imposed to keep the computation going.

In the code-implementation of the SSA, we apply a nested approach to avoid calculating all of the individual probabilities associated with the events in Table 1 unless deemed necessary [24]. As an example, consider two assemblies with fast neutron sources S^1_1 and S^2_1 and total transition rates for group g: $\lambda^1_{t,g}$ and $\lambda^2_{t,g}$. We call the probability per unit time that a source event occurred $P_S = S^1_1 + S^2_1$ and the probability per unit time that a neutron interaction occurred $P_N = \sum_j \sum_g n_{g,j}\lambda^j_{t,g}$, then $\mu = P_S + P_N$. We then compare a random number ξ to determine which of two criteria is satisfied: if $\xi \in [0, P_S/\mu]$, then a source event occurs otherwise a neutron interaction occurs. The assembly in which the event occurs is then obtained as follows. If a source event occurs in assembly 1, the criteria (with a different ξ) $\xi \in [0, S^1_1/P_S]$ is satisfied, otherwise $\xi \in (S^1_1/P_S, 1]$ is true and the source event occurs in assembly 2. Once the assembly is known, we then sample the number of fast neutrons emitted in the event using the appropriate CDF of the source multiplicity distribution and update $n_{1,j} \rightarrow n_{1,j} + \nu$.

If a neutron induced event occurs, we first decide in which assembly the event occurred by checking which criteria is satisfied by a new random number: $\xi \in [0, (\sum_g n_{g,1}\lambda^1_{t,g})/P_N]$ for assembly 1 otherwise $\xi \in ((\sum_g n_{g,2}\lambda^2_{t,g})/P_N, 1]$ and the event occurs in assembly 2. For the known assembly, say assembly j', we define $P_{N,j'} = \sum_g n_{g,j'}\lambda^{j'}_{t,g}$, then the energy group the neutron causing the event is determined by comparing $\xi \in [0, n_{1,j'}\lambda^{j'}_{t,1}/P_{N,j'}]$ for group 1 or $\xi \in (n_{1,j'}\lambda^{j'}_{t,1}/P_{N,j'}, 1]$ for group 2. From there, the event that occurs is determined by sampling another ξ for the known energy group g': $\xi \in [0, \lambda^{j'}_{c,g'}/\lambda^{j'}_{t,g'}]$ for capture; $\xi \in (\lambda^{j'}_{c,g'}/\lambda^{j'}_{t,g'}, (\lambda^{j'}_{c,g'} + \lambda^{j'}_{f,g'})/\lambda^{j'}_{t,g'}]$ for an induced fission; or $\xi \in ((\lambda^{j'}_{c,g'} + \lambda^{j'}_{f,g'})/\lambda^{j'}_{t,g'}, 1]$ for a leakage event. For a capture event, simply update the population as $n_{g',j'} \rightarrow n_{g',j'} - 1$; for an induced fission, assuming that only thermal neutrons induce fission, we sample from $q^{f,j'}_{\nu,2}$ to find ν fast neutrons emitted, and update the population as $n_{1,j'} \rightarrow n_{1,j'} + \nu$ and $n_{2,j'} \rightarrow n_{2,j'} - 1$; and for leakage, we say $n_{g',j'} \rightarrow n_{g',j'} - 1$, and if there is a successful transfer to assembly k, we update $n_{g',k} \rightarrow n_{g',k} + 1$. Our system is now in state $\mathbf{n}'$, and we then sample the time interval to the next event and update $\mu(\mathbf{n}', t')$ using the updated populations to once again repeat the process until a stopping criteria is satisfied.

The neutron number pdf, which is the quantity of interest, is computed by averaging over histories. For a given history, or simulation, there will be a single outcome, or state, that the system occupies. The final

state of history h will have a corresponding neutron population, $\mathbf{n}_h$, at the final time of observation, t_f; this state is defined as $(\mathbf{n}_h, t_f)$ with unit magnitude: $|(\mathbf{n}_h, t_f)|$. The probability of there being $\mathbf{n}$ neutrons at the final time, then, is simply the total number of instances that state occurs divided by the total number of histories simulated, H, given by

$$P_{\mathbf{n}}(t_f) = \frac{1}{H} \sum_{h|\mathbf{n}_h=\mathbf{n}} |(\mathbf{n}_h, t_f)|\,, \tag{27}$$

where the above is read as the sum over h conditioned on $\mathbf{n}_h = \mathbf{n}$. In practice, the summation of Eq. 27 is accomplished by populating a histogram for every outcome on-the-fly, preventing the need to store every outcome as an individual value in a computer.

As the FME (or the generating function equation) is intractable to exact solution except under highly simplified conditions, it is not feasible to benchmark or verify the neutron number distribution obtained from the SSA algorithm in this strict sense, although SSA and single event Monte Carlo yield identical solutions, within statistics. However, by comparing the SSA mean and variance against those obtained from numerical solution of the moment equations, a limited benchmark can be achieved, which at least ensures consistency of these parameters between the gamma distribution and the SSA number distribution. The moment comparisons are shown below, but first we describe how the point kinetic parameters were obtained.

4. Point Kinetics Parameters and Nuclear Data

In this section, we describe the calculation of the assembly parameters used in the SSA simulation and the deterministic moment calculations. We also present problem specifications and nuclear data for the ensuing computational scenarios.

4.1. Point Kinetics Parameters

The point kinetics parameters - reaction rates and neutron lifetime - are calculated for an isolated 1D spherically symmetric assembly using the standard adjoint-weighted methodology [26]. We have neglected neutron exchange between assemblies in the calculation of point kinetic parameters, which is clearly an approximation and one that can presumably be relaxed by generalizing the standard adjoint projection approach (this topic appears to not have received much attention in the literature). This limitation does not, however, restrict the validity of the present investigation as the same parameters will be used in both the SSA and moment calculations. That is, differences between the two approaches cannot be attributed to the use of approximate transition probabilities.

Forward and adjoint k-eigenvalue calculations were performed by solving the two-group, spherically symmetric isotropic scattering transport equation with vacuum boundary conditions, using discrete ordinates in angle, diamond difference discretization in space, and source- and power-iteration [25] to obtain the k-eigenvalues and the fundamental modes $\psi_{g,j}(r,\mu)$ and $\psi^{\dagger}_{g,j}(r,\mu)$. The adjoint-weighted total neutron population in group g and assembly-j is then obtained from [26]

$$N^j_g = \int_0^{R_j} \mathrm{d}r\, r^2 \int_{-1}^{1} \frac{\mathrm{d}\mu}{2}\, \psi^{\dagger}_{g,j}(r,\mu) \frac{1}{v_g} \psi_{g,j}(r,\mu) \tag{28}$$

where R_j is the radius of assembly-j, and the capture/fission and leakage rates by

$$R^j_{\zeta,g} = \int_0^{R_j} \mathrm{d}r\, r^2 \int_{-1}^{1} \frac{\mathrm{d}\mu}{2}\, \psi^{\dagger}_{g,j}(r,\mu) \Sigma^j_{\zeta,g} \psi_{g,j}(r,\mu) \tag{29a}$$

$$R^j_{\ell,g} = 4\pi R_j^2 \int_0^{1} \mathrm{d}\mu\, \psi^{\dagger}_{g,j}(R_j,\mu) \mu \psi_{g,j}(R_j,\mu), \tag{29b}$$

where $\zeta = \{c, f\}$ for fission or capture and the sum of these rates is denoted by $R^j_{t,g}$. The mean time between reactions of type y for neutrons of energy group g in assembly-j, $\tau^j_{y,g}$, is defined as

$$\tau^j_{y,g} = \frac{N^j_g}{R^j_{y,g}}, \tag{30}$$

Table 2: Data used for the two sphere system.

(a)

Energy $[eV]$	σ_f $[b]$	σ_c $[b]$	σ_s $[b]$	v $\left[\frac{cm}{s}\right]$
$14 \cdot 10^6$	2.053	$889.7 \cdot 10^{-6}$	2.839	$5.175 \cdot 10^9$
0.0253	585.1	98.71	15.12	$2.200 \cdot 10^5$

(b) $\sigma_{s,g\to g'}$, $[b]$.

g \ g'	1	2
1	1.5376	1.3014
2	0.0	15.12

Table 3: Multiplicity distributions.

	$\overline{\nu}$	$\overline{\nu^2}$	q_ν							
			0	1	2	3	4	5	6	7
$g = 1$, IF	4.458	21.29	0.0	0.009	0.022	0.179	0.310	0.310	0.112	0.058
$g = 2$, IF	2.476	7.382	0.022	0.200	0.306	0.307	0.136	0.035	0.004	0.0
SF	2.154	5.945	0.0638	0.2316	0.3325	0.2533	0.0987	0.0181	0.0020	0.0

with

$$\frac{1}{\tau_g^j} = \sum_y \frac{1}{\tau_{y,g}^j}, \tag{31}$$

while the reciprocal gives the transition probability (per unit time) of neutron in group g and assembly-j undergoing a collision of type-y:

$$\lambda_{y,g}^j = \frac{1}{\tau_{y,g}^j}. \tag{32}$$

4.2. Problem Specification and Data

For numerical implementation, we consider two spherical assemblies composed of pure ^{235}U metal with radii R_1 and R_2 and a number density of $N = 5.0884 \cdot 10^{-2}$ $(b \cdot cm)^{-1}$. Table 2 displays the two-group microscopic cross section data at 300 K for both assemblies obtained from the `JENDL`-4.0 library. These cross sections will be used unless otherwise specified for the few instances where we need to ignore certain interactions for benchmarking purposes or for developing our understanding of the systems. Data for the neutron multiplicity distribution for induced fission (IF) and spontaneous fission (SF) is displayed in Table 3, where g refers to the particle emission distribution due to a neutron of energy group g inducing said fission. We note that the IF distributions are not normalized, but initial tests showed that the neutron number distributions are not noticeably different due to this issue. When calculating the moments of the number distribution, we use the first two factorial moments, $\overline{\nu}$ and $\overline{\nu(\nu-1)}$, and we use the actual emission probabilities when randomly sampling fission event outcomes in the SSA code.

For specificity, the center of assembly-1 is located at the origin such that $\vec{C}_1 = \langle 0, 0, 0\rangle$, while assembly-2 has a center located a distance $L = R_1 + S + R_2$ along the y-axis (S is the shortest distance between the two surfaces), giving $\vec{C}_2 = \langle 0, L, 0\rangle$. The distance between the sphere surfaces is set to $S = 5.0$ cm and the view factor method [14] is used to compute the transfer probabilities according to

$$p_{j\to k} = \left(\frac{\mathcal{Q}}{\mathcal{R}}\right)^2 \left[1 - \sqrt{1 - \left(\frac{\mathcal{R}}{\mathcal{Q}}\right)^2}\right] \left[1 - \sqrt{1 - \left(\frac{1}{\mathcal{Q}}\right)^2}\right], \tag{33}$$

Table 4: Transfer probabilities.

Configuration	$p_{1\to 2}$	$p_{1\to\infty}$	$p_{2\to 1}$	$p_{2\to\infty}$
1	$1.2376 \cdot 10^{-2}$	0.98762	$8.8879 \cdot 10^{-3}$	0.99111
2	$7.7398 \cdot 10^{-3}$	0.99226	$5.6483 \cdot 10^{-3}$	0.99435

Table 5: Parameters for Configuration 1. Reaction rates have units of s^{-1}.

Assembly	R_j $[cm]$	$k_{eff,j}$	τ_j	$\lambda_{f,j}$	$\lambda_{c,j}$	$\lambda_{\ell,j}$
1	5.9	1.0035	0.7741 ns	$5.406 \cdot 10^8$	$2.343 \cdot 10^5$	$7.509 \cdot 10^8$
2	5.0	0.8788	0.6584 ns	$5.406 \cdot 10^8$	$2.343 \cdot 10^5$	$9.779 \cdot 10^8$

where $\mathcal{Q} = \mathcal{R} + \mathcal{S} + 1$, $\mathcal{R} = R_j/R_k$, and $\mathcal{S} = S/R_k$. Additional transfer probabilities are given by:

$$p_{k\to j} = \mathcal{R}^2 p_{j\to k} \tag{34a}$$

$$p_{j\to\infty} = 1 - p_{j\to k} \tag{34b}$$

$$p_{k\to\infty} = 1 - \mathcal{R}^2 p_{j\to k}. \tag{34c}$$

Numerical values are given in Table 4 for the two configurations to be investigated, as detailed below. Note that the selection of $S = 5.0$ cm was deliberate as it is the closest point these two spheres may be for which the view factor will still be relatively accurate [14].

For single-chain simulations, we assume that the initiating neutron appears in assembly-1 at $t = 0$. For problems with sources, we need not differentiate systems based on initial neutron population as the initial condition is nonunique: $P_{\mathbf{n}}(0) = \delta_{n_1,0}\delta_{n_2,0}$. Also, we assume that the reaction rates are time-independent except in Sec. 6.4, where we simulate a dynamic reactivity scenario.

4.2.1. Configuration 1: Two Assemblies with Monoenergetic Fast Neutrons

In this configuration, only monoenergetic fast neutrons are considered in both assemblies with the fast group data given in Table 2a. The assemblies are identical in composition but have different radii, $R_1 = 5.9$ cm and $R_2 = 5.0$ cm, such that taken in isolation assembly 1 is slightly supercritical with $k_{\text{eff}} = 1.0035$ and assembly 2 subcritical with $k_{\text{eff}} = 0.8788$. The neutron lifetime and the reaction rates appropriate for single energy neutrons are summarized in Table 5 while Table 6 gives the relevant internal source data.

4.2.2. Configuration 2: Two Assemblies with Fast and Thermal Neutrons

In this configuration, both fast and thermal neutron populations are considered, with assembly parameters given in Table 7 based on two group data from Table 2 that includes group transfer due to scattering. In order to maintain the same k_{eff} values at the 5 cm separation distance, the sphere radii were altered to $R_1 = 2.484$ cm and $R_2 = 2.122$ cm. Changing the sizes only causes meaningful change between the (fast) leakage rate and lifetime, where we see that the leakage rate increases while the lifetime decreases when the assembly is reduced in size. Source neutrons are assumed to be emitted in the fast group only, with strengths shown in Table 6.

5. Moment Benchmarking

As the moments of the distributions uniquely determine the gamma distribution for the neutron number pdfs, we briefly discuss the numerical solution of the moments for Configuration 1 described in Sec. 4.2.

Table 6: Neutron source data for Configuration 1.

Assembly	Volume $[cm^3]$	S_j $[1/s]$	S_j/V_j $[1/(cm^3 \cdot s)]$
1	860.3	10^6	1,162.4
2	523.6	10^6	1,909.6

Table 7: Parameters for Configuration 2. Reaction rates have units of s^{-1}.

(a)

Assembly	R_j $[cm]$	$k_{eff,j}$	Group	τ_g^j	$\lambda_{f,g}^j$	$\lambda_{c,g}^j$	$\lambda_{\ell,g}^j$
1	2.484	1.0035	1	0.1753 ns	$5.406 \cdot 10^8$	$2.343 \cdot 10^5$	$4.820 \cdot 10^9$
–	-	-	2	3.982 ms	214.4	36.16	0.5889
2	2.122	0.8788	1	0.1445 ns	$5.406 \cdot 10^8$	$2.343 \cdot 10^5$	$6.039 \cdot 10^9$
–	-	-	2	3.980 ms	214.4	36.16	0.7268

(b) Scattering reaction rates

$\lambda_{s,g\to g'}^1$			$\lambda_{s,g\to g'}^2$		
g \ g'	1	2	g \ g'	1	2
1	$4.049 \cdot 10^8$	$3.427 \cdot 10^8$	1	$4.049 \cdot 10^8$	$3.427 \cdot 10^8$
2	0.0	5.5395	2	0.0	5.5395

Although the SSA method was previously benchmarked against analytical solutions obtained under simplified assumptions, the comparison of the SSA moments against the deterministically computed moments provides a partial benchmarking of the SSA algorithm under the more general conditions of this investigation. The system of moment ODEs are solved by a modified divided difference form of the Adams PECE formulae and local extrapolation, adjusting the order and step size to control the local error per unit step [27]. (Numerical details along with more extensive benchmarking can be found in [28])

For Configuration 1, only the fast group components of the moment equations given in Sec. 2.1. are solved. The SSA results were obtained by setting the final time to some scaled value of the neutron lifetime in assembly 1 and running 10^3 batches each with 10^5 histories, amounting to 10^8 total simulations per reported final time, resulting in highly converged confidence intervals. The deterministically computed mean and standard deviation of the neutron number are compared against corresponding SSA results in Fig. 1 for (a) a single neutron chain with the initial populations being $N_1 = 1$ and $N_2 = 0$, and (b) for the case where both assemblies have sources of $S = 10^6$ $1/s$ and the initial condition being $N_1 = N_2 = 0$. Note that, although $S = 10^6$ $1/s$ seems like a strong source, the intrinsic η (i.e., non-fitted η given by Eq. 20, rather than Eq. 24) is $\eta = 9.7 \cdot 10^{-4}$, meaning these assemblies are classified as having a weak source and the neutron population is strongly stochastic. Recall from Table 7a that assembly 1 is slightly supercritical with $k_{\text{eff}} = 1.0035$ while assembly 2 is subcritical with $k_{\text{eff}} = 0.8788$, so that in isolation the mean neutron number in assembly 1 will eventually diverge while that in an isolated assembly 2 will vanish. In addition to showing the excellent agreement between the SSA and deterministically computed moments, the figure demonstrates the effectiveness of coupling, even with less than 1% transfer probability between the assemblies. The time variation of the moments of the subcritical assembly follow the trend of the moments of the supercritical assembly within 20 lifetimes, showing that the supercritical system dominates the behavior of the assemblage.

6. Numerical Results for Number Distributions

We now compare neutron number pdfs computed from the gamma distribution and SSA simulations under different conditions.

6.1. Configuration 1: Isolated Assembly

We first consider an isolated assembly and establish the accuracy of the gamma distribution in describing the stochastic state under sub- and supercritical conditions. All of the SSA results were obtained by simulating $5,000$ batches with 10^7 histories per batch. The η_j parameter of the gamma distribution was obtained by numerically solving the deterministic moment equations and using Eq. 24. Converging the stochastic simulation to within a prescribed small standard deviation was not practical for computing the neutron number probability distributions, especially for large neutron numbers that are associated with

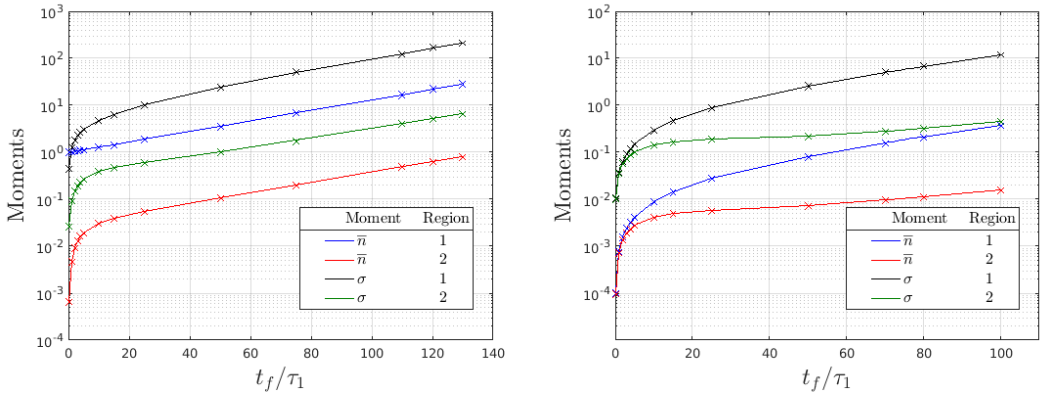

Figure 1: Comparison of the SSA (x) moments with the numerical solution (-) of the moment ODEs for (a) the single chain and (b) with a source.

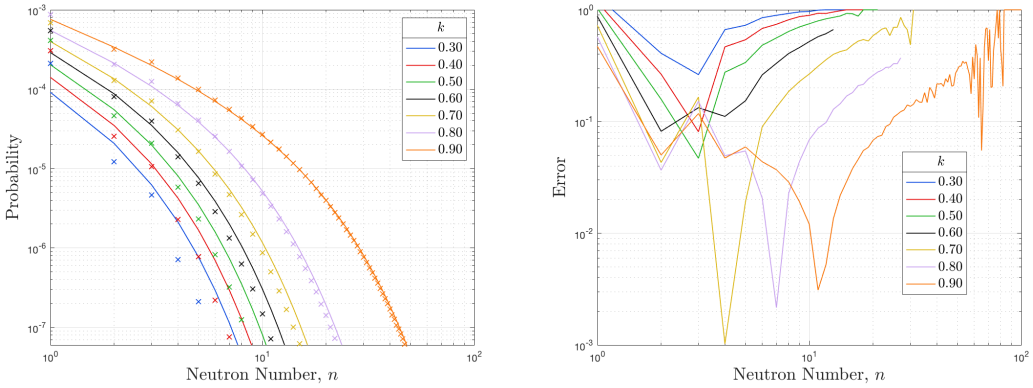

Figure 2: (a) Fast neutron number distributions in a subcritical assembly of varying criticality as calculated by SSA (x) and the gamma distribution fit (solid lines) and (b) the relative error between the two distributions.

low probabilities. However, conclusive comparisons for the bulk of the distribution can be made within the achieved accuracy.

Figure 2a shows the steady state SSA and gamma number distributions in a subcritical assembly with k in the range $(0.3, 0.9)$ and an intrinsic source strength $S = 10^6\ 1/s$, while Figure 2b shows the corresponding relative error. The gamma distribution becomes increasingly representative of the neutron distribution with increasing multiplication, except for neutron numbers of $\mathcal{O}(1)$, where the distribution is invalid. Although the deviation appears to increase markedly at higher neutron numbers, the absolute value of the probabilities is small and the associated statistical noise significant. The corresponding results for a supercritical system with $k = 1.0035$ are displayed in Fig. 3a for varying times (scaled by the fast neutron lifetime). The distribution rapidly approaches the gamma distribution (within 10 lifetimes) with the relative accuracy increasing as the population size grows, in accordance with the asymptotic criteria that the mean has grown sufficiently large and $t \gg \tau$, the neutron lifetime.

At a glance, the supercritical system agrees with a gamma distribution within 10 lifetimes while the

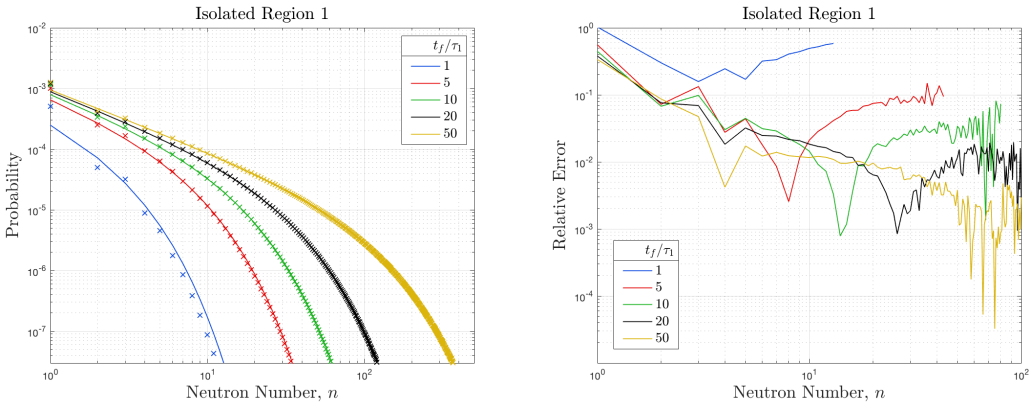

(a) (b)

Figure 3: (a) Neutron number distribution at varying times in supercritical assembly with $k = 1.0035$. (b) relative error between the SSA pdf and the gamma fit

distribution of the subcritical assembly reaches steady-state within 50 lifetimes. Figures 2b and 3b display the respective relative error counterparts to the distributions of Figs. 2a and 3a. For the subcritical cases, we see the bulk of the relative error decreases for increasing k. For the $k = 0.90$ case, the relative error is between 1% and 10% for the entire distribution (note the error begins increasing at the tail due to poor statistical resolution). For the supercritical case, we see the error decreases as time progresses and the mean of the population increases. Within 10 lifetimes, the MC and fitted distributions agree within 10% and by 50 lifetimes, the distributions agree within 0.1% - 1%.

6.2. Configuration 1: Two Coupled Assemblies

We now consider the population behavior when the two assemblies are brought within 5.0 *cm* of each other. Figure 4 shows the comparison between the neutron number pdf as calculated by SSA as well as the fitted gamma distribution.

We see that the supercritical assembly 1 in Fig. 4a visually appears indistinguishable from the distributions of Fig. 3a. It would appear that the introduction of the additional fuel from assembly 2 has little effect on the dynamic behavior of assembly 1. On the other hand, the subcritical assembly 2 shows a drastic difference in behavior, when comparing Fig. 2a with Fig. 4b; that is to say that the distribution in the subcritical system no longer reaches a steady-state, but instead behaves dynamically with an increasing mean. For a more rigorous comparison, Figs. 5a and 5b show that the relative error between the SSA and fitted gamma distributions. Mirroring the above observation of assembly 1, the error profiles over time appear practically identical as those in Fig. 3b. We see in Fig. 5 that the subcritical error falls to 10^{-2} at $n = 100$ around 100 lifetimes. From this, it is clear that the addition of the other assembly is equivalent to adding multiplying mass or a source to a single system and will drive the other assembly to achieve a gamma distribution. Although assembly 2 itself remains subcritical, the transfer of the leaked particles from assembly 1 is enough to force the population to continually increase. This driving of the collective system population is expected to increase indefinitely as long as assembly 1 remains supercritical. Finally, we note that the inherent Monte Carlo statistical noise is inevitably observed in the error plots for increasing n and, once it begins to dominate, the decreasing trend in the error profile is reversed.

6.3. Configuration 2: Two Coupled Assemblies with Fast and Thermal Neutrons

We allow for fast and thermal induced fission using the cross section data of Table 2. Group-dependent reaction rates are displayed in Table 7, where we altered the system sizes to radii of $R_1 = 2.484$ *cm* and $R_2 = 2.122$ *cm* such that the effective multiplication factors are the same as before; as expected, the critical

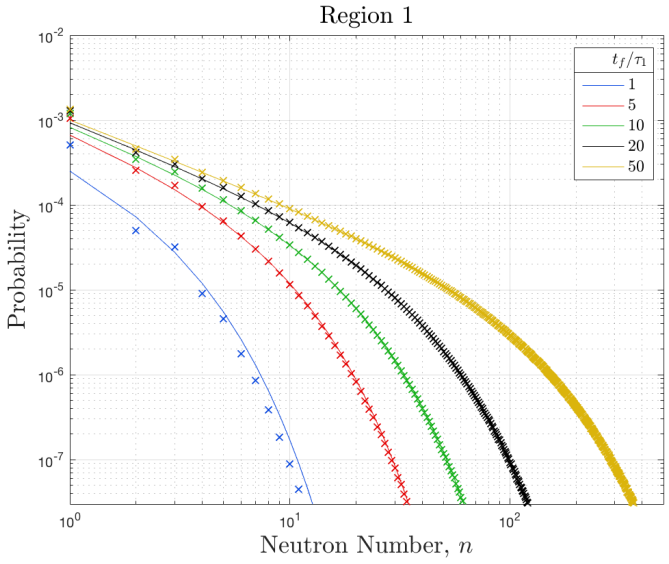

(a)

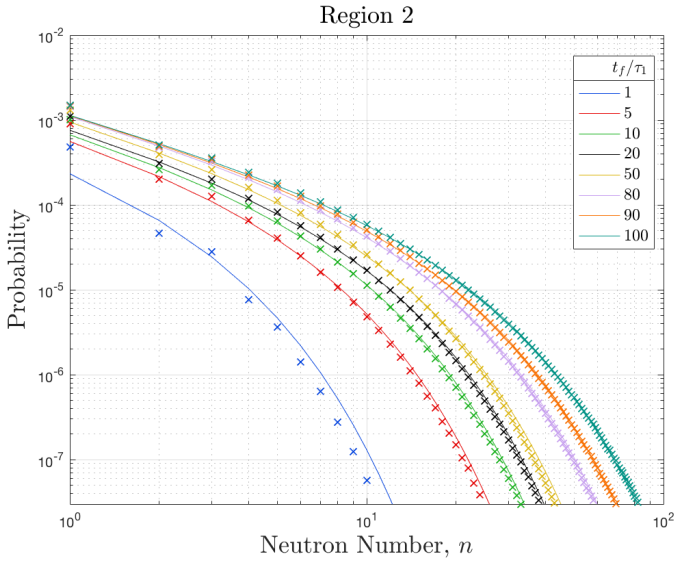

(b)

Figure 4: Comparison of the neutron number pdfs as calculated by SSA (x) and the gamma distribution fit (-) for (a) assembly 1, (b) assembly 2.

mass substantially decreases when induced fission from fast and thermal neutrons is accounted for (compared to the $R_1 = 5.9\ cm$ from before). By spatially coupling the two assemblies and separating them by 5.0 cm, we demonstrate the convergence of the energy-dependent neutron number pdfs for fast neutron source-driven systems. The timescales worth considering are on the order of the thermal neutron lifetime (for which we choose assembly 1 with $\tau_2^1 = 3.982\ ms$).

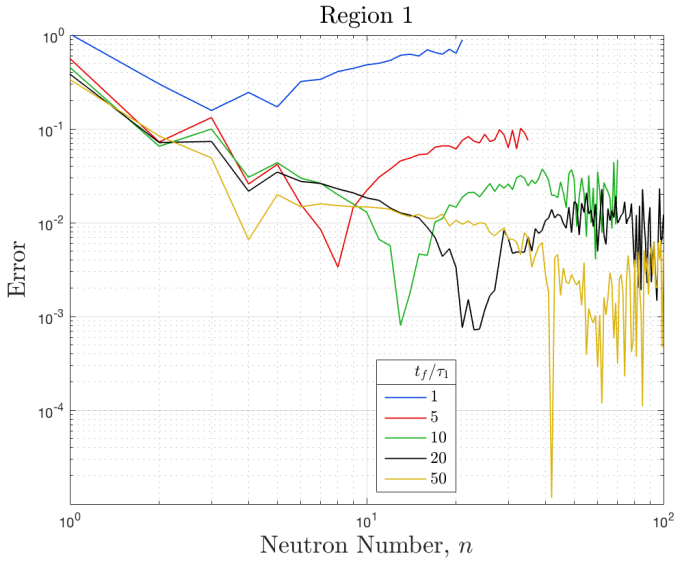

(a)

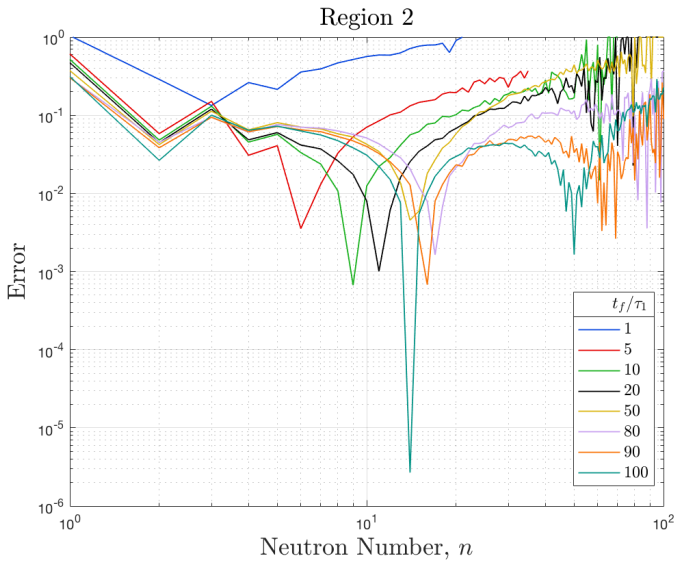

(b)

Figure 5: Per Fig. 4, but for the relative error between the SSA and gamma fit for (a) assembly 1 and (b) assembly 2.

Figure 6 depicts the neutron number pdfs in the two-assembly setup at different times for fast neutrons in 6a and thermal neutrons in 6b; also included are the fitted gamma distributions (dotted lines) and, for the thermal neutron pdfs, additional fitted Gaussian distributions (solid lines). All distributions have the same mean and variance per the methods outlined in Sec. 2.2. From Fig. 6, we see that the stochastic (weak) fast neutron sources give rise to unimodal thermal neutron distributions, which behave like strong stochastic sources with a shape parameter greater than one, within 5 thermal neutron lifetimes.

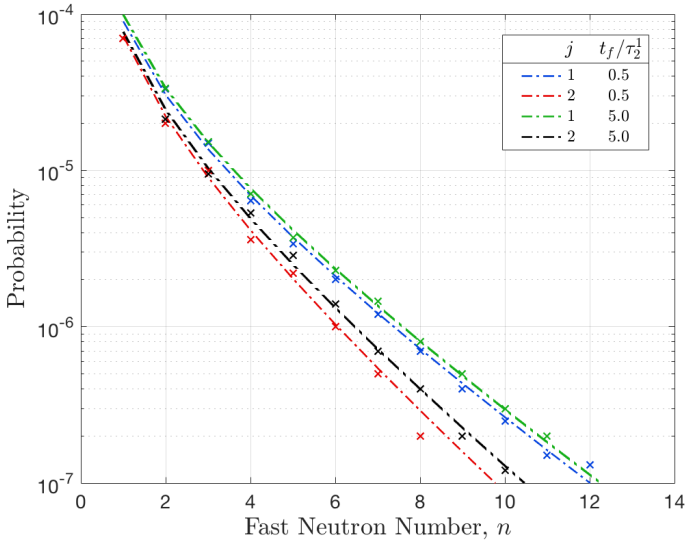

(a)

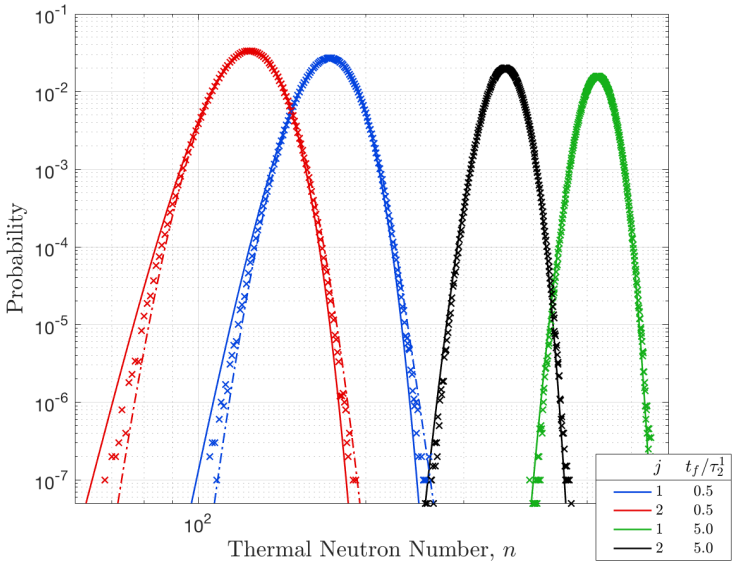

(b)

Figure 6: Neutron number pdfs in a two-assembly assembly at different times for (a) fast neutrons and (b) thermal neutrons. The xs are SSA results, solid lines are Gaussian fits, and dotted lines are Gamma fits.

The fast neutron pdfs of Fig. 6a remain stochastic in nature- that is to say, the distributions are monotonically decreasing. Although fast neutrons originate from fast fission, thermal fission, and source events, the persistence of stochastic behavior of the fast neutron population is due to the abrupt disappearance of these neutrons either by reacting with the medium or leakage. Strong down-scattering to the thermal regime causes

an accumulation in the thermal neutron population because the thermal neutrons are much slower-moving, consistent with the fast and thermal reaction rate values in Table 7.

We also observe the thermal neutron pdfs in Fig. 6b are not quite in agreement with a gamma distribution fit (dotted lines) at an early time of $t_f = 0.5\tau_2^1$, but are indeed bounded between a gamma fit and a Gaussian fit (solid lines). At a later time of $t_f = 5\tau_2^1$, the true thermal pdf is in agreement with a fitted Gaussian distribution and the gamma has converged onto this distribution as well. This is the expected asymptotic behavior of the gamma distribution, in general, in accordance with the Central Limit Theorem [29]. The shape parameter in this case is η, given by Eq. 24, which states that as the variance decreases, η increases, which causes the observed convergence. From a physical standpoint, the early-time difference from the gamma fit is most likely due, in part, to the fast fission events causing large bursts of fast neutrons (compare the fast and thermal multiplicity distributions in Table 3) which quickly down-scatter; this will cause the true pdf to have different higher order moments (e.g., skewness and kurtosis) than the fitted gamma, causing the departure from the fitted gamma to the fitted Gaussian.

6.4. Time-Dependent Reactivity

In this section, we consider the effect of coupling when the reactivity in assembly 1 is allowed to vary with time, to simulate, for instance, a burst reactor in the vicinity of a subcritical assembly. The SSA simulation and moment calculations are adapted for a specified time varying reactivity in assembly 1 while assembly 2 is held in a static subcritical state.

We assume a polynomial in time reactivity variation for assembly 1 of the form:

$$\rho_1(t) = \rho_1(0) + \sum_{m=1}^{M} a_{1,m} t^m, \tag{35}$$

where $\rho_1(0)$ is the initial value of the reactivity in assembly 1 and $a_{1,m}$ are known coefficients. Note the reactivity equation for assembly 2 is simply $\rho_2(t) = \rho_2(0)$; thus, $a_{2,m} \equiv 0$. The mean generation time for neutrons in $(g,1)$ is $\Lambda_g^1 = \tau_g^1/k_1$ and we note $\lambda_{t,g}^1 = 1/\tau_g^1$ and $k_1 = 1/(1-\rho_1)$. From this, we may rewrite μ of Eq. 26 in terms of the time-dependent assembly-collective reactivity:

$$\mu(\mathbf{X}, t) = \sum_{j=1}^{J=2} \sum_{g=1}^{G=2} \left\{ S_g^j + \left[\frac{1-\rho_j(t)}{\Lambda_g^j} \right] n_{g,j} \right\}. \tag{36}$$

The cumulative distribution function for the time to next event is given by

$$\begin{aligned} F(t) &= \int_0^t \mathrm{d}t' \mu(\mathbf{X}, t') \exp\left\{ -\int_0^{t'} \mathrm{d}t'' \mu(\mathbf{X}, t'') \right\} \\ &= 1 - \exp\left\{ -\int_0^t \mathrm{d}t' \mu(\mathbf{X}, t') \right\}, \end{aligned} \tag{37}$$

which, upon inserting Eqs.(35) and (36), gives:

$$\int_0^t \mathrm{d}t' \mu(\mathbf{X}, t') = \sum_{j=1}^{2} \sum_{g=1}^{2} \left[S_g^j + \left(\frac{1-\rho_j(0)}{\Lambda_g^j} \right) n_{g,j} \right] t - \sum_{g=1}^{2} \frac{n_{g,1}}{\Lambda_g^1} \sum_{m=1}^{M} \frac{a_{1,m}}{m+1} t^{m+1}, \tag{38}$$

where we used $a_{2,m} \equiv 0$. Finally, setting $F(t) = \xi$ where $\xi \sim U(0,1)$ yields, from Eq. 37, the following polynomial for the time to the next event:

$$\sum_{m=1}^{M} A_m t^{m+1} + Bt + C = 0, \tag{39}$$

with the coefficients defined as

$$A_m = \frac{a_{1,m}}{m+1}\sum_{g=1}^{G}\frac{n_{g,1}}{\Lambda_g^1}$$
$$B = -\sum_{g=1}^{G}\sum_{j=1}^{J}\left[S_g^j + \left(\frac{1-\rho_j(0)}{\Lambda_g^j}\right)n_{g,j}\right]$$
$$C = = -\ln(1-\xi) = -\ln\xi.$$

The time of the next event, t, is determined by finding the principle root of Eq. 39 for a sampled ξ. For numerical illustration we consider a linear ramp reactivity variation in assembly 1, which follows upon setting $M = 1$:

$$\rho_1(t) = \begin{cases}\rho_1(0) + \Delta\rho_1\frac{t}{t_{in}}, & t \le t_{in}\\ \rho_{1,\max}, & t \ge t_{in}\end{cases} \tag{40}$$

where t_{in} is the time of maximum reactivity insertion, $\rho_1(t_{in}) = \rho_{1,\max}$, $\Delta\rho_1 = \rho_{1,\max} - \rho_1(0)$ and $a_{1,1} = \Delta\rho_1/t_{in}$. From this, Eq. 39 reduces to a quadratic polynomial with the roots

$$t = -\frac{B}{2A_1} \pm \frac{1}{2A_1}\sqrt{B^2 - 4A_1C}, \tag{41}$$

where A_1 is given by:

$$A_1 = \frac{\Delta\rho_1}{2t_{in}}\sum_g\frac{n_{g,1}}{\Lambda_g^1} = \frac{1}{2t_{in}}\sum_g\left(\lambda_{t,g}^1(0) - \lambda_{t,g}^1(t_{in})\right)n_{g,1}. \tag{42}$$

The linear reactivity variation is modeled by allowing the material density of assembly 1 to have an appropriate time dependence while keeping the radius and cross-sections constant and all properties of assembly 2 constant. We set the initial reactivity to $\rho_1(0) = \rho_{o,1} = -1.0$, and the final reactivity at t_{in} to $\rho_1(t_{in}) = \rho_{1,\max} = 0.\overline{0909}$, giving $k_{\text{eff},1}(0) = 0.50$ to $k_{\text{eff},1}(t_{in}) = 1.10$. The constant criticality of assembly 2 is $k_{\text{eff},2} = 0.8788$ which corresponds to a reactivity of $\rho_2 = -0.1379$.

For the previously used microscopic cross-sections, the initial density must be $\varrho(0) = 9.02221825\ g/cm^3$ and the final density must be $\varrho(t_{in}) = 22.21289\ g/cm^3$. Solving the k-eigenvalue neutron transport equation for every integer value of density between these two values gives an array of 15 $k_{\text{eff},1}$ values. For a given $k_{\text{eff},1}$, we calculate the reactivity with $\rho_1(k_{\text{eff},1}) = 1 - 1/k_{\text{eff},1}$, and we then determine the corresponding time using $t = t_{in}[\rho_1(k_{\text{eff},1}) - \rho_1(t=0)]/\Delta\rho$. From this, we then perform a least-squares fit to the data points using MATLAB's polyfit function. Figure 7 shows the data values ($\circ$ and x markations) and the fourth-order polynomial fit lines for k_{eff} and ϱ out to a $t_{in} = 0.5\tau_2^1(0)$. Table 8 presents the coefficients for the polynomial fits of the functional form:

$$f(t) = c_4t^4 + c_3t^3 + c_2t^2 + c_1t + c_0, \tag{43}$$

that we will then use to update our reaction rates and other values in the SSA code for time interval sampling. Note that, if t_{in} is altered for a given $\Delta\rho$, one must refit the polynomials. The coefficient tables are given in Table 8 for two other t_{in} values.

The severity of the reactivity insertion in assembly 1 can be controlled by varying the final time of the reactivity insertion, t_{in}. Figure 8 shows the reactivity profile corresponding to the density profile in Fig. 7 along with two additional, more severe, profiles that we will investigate.

Figure 9a shows the fast neutron population pdfs at the end of the respective insertions, depicted in Fig. 8, for assembly 1; we do not show the fast pdfs for assembly 2 as the means are so low and seem to be constant values of $\overline{n}_{1,2}(0.01\tau_2^1(0)) \approx 1.87\cdot10^{-4}$, $\overline{n}_{1,2}(0.1\tau_2^1(0)) \approx 1.30\cdot10^{-4}$, and $\overline{n}_{1,2}(0.5\tau_2^1(0)) \approx 1.50\cdot10^{-4}$. Figure 9b shows the thermal neutron number pdfs for both assemblies at the end of the respective reactivity insertions. As was shown before, we compare the SSA (true) results with a gamma distribution and Gaussian distribution by matching the moments, where it is clear that the SSA result is always bounded by the fitted distributions. Interestingly, the assembly 1 fast neutron pdfs agree perfectly with the fitted gamma distribution (the x's

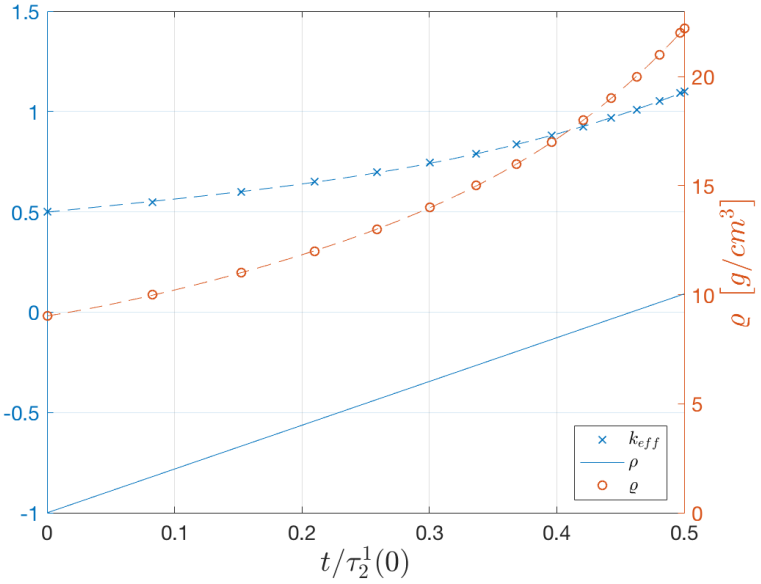

Figure 7: Time dependent assembly 1 density, multiplication factor, and reactivity data (∘ and x points) compared with polynomial fits (dashed lines) used in SSA code.

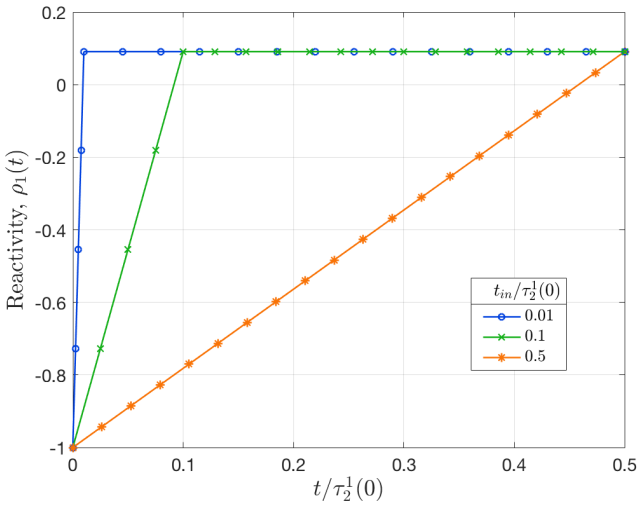

Figure 8: Reactivity insertion profiles of differing severity.

lie atop the dotted gamma fit line), while the thermal neutron pdfs converge to the Gaussian fitted line (for which the gamma has converged to as well due to smaller variances), even though the populations are smaller than their fast counterparts. We note that at the earlier time of $t_{in} = 0.01\tau_2^1(0)$, although assembly 1 is the assembly experiencing the reactivity insertion, it is assembly 2 that has a larger thermal neutron population average. This is most likely due to the increase in the neutrons leaking, specifically fast neutrons, from assembly 1 which then transfer to the other assembly.

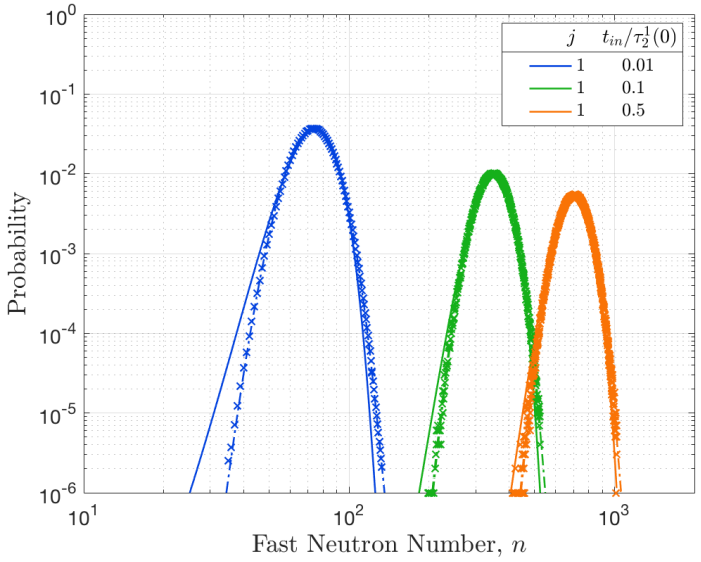

(a)

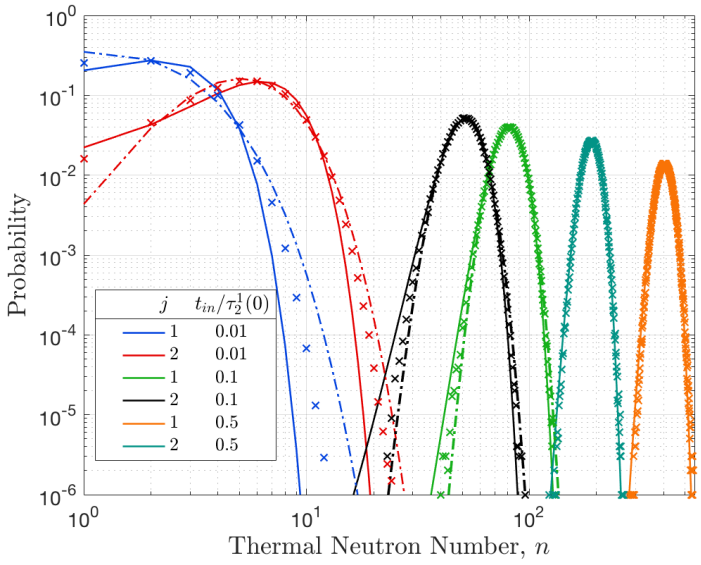

(b)

Figure 9: Neutron population pdfs at the end of several reactivity insertions (i.e. $t = t_{in}$) in assembly 1 for (a) fast neutrons and (b) thermal neutrons. xs are SSA results, solid lines are Gaussian fits, and dotted lines are Gamma fits.

We now complete the simulations by running past the insertion times to a common final time of $t_f = 0.5\tau_2^1(0)$, in reference to the assembly 1 reactivity profiles of Fig. 8. In the SSA code, once the system time surpasses the prescribed t_{in}, the reaction rates are held constant at their max values occurring at the end of the insertion. Illustrated in Fig. 10 are the corresponding energy-dependent neutron number distributions

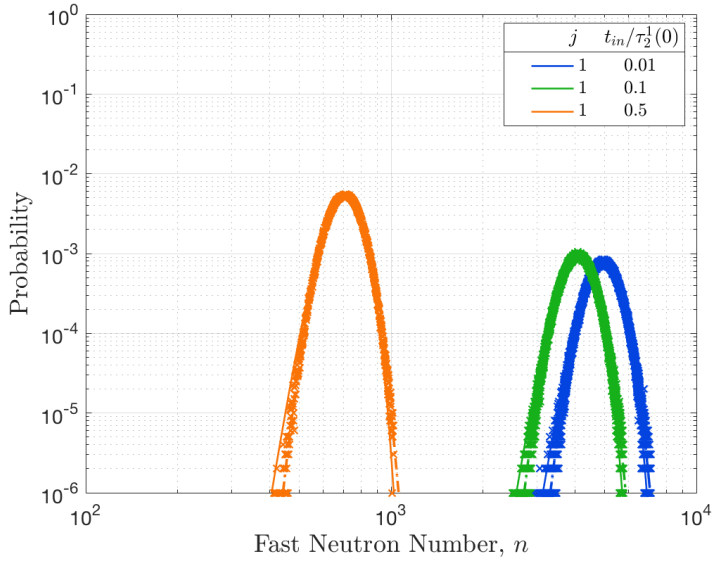

(a)

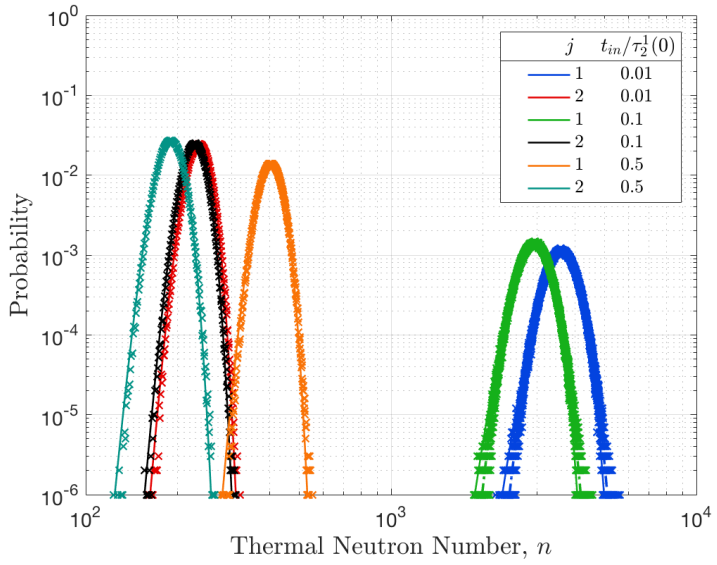

(b)

Figure 10: Per Fig. 9, to later times. xs are SSA results, solid lines are Gaussian fits, and dotted lines are Gamma fits.

for fast neutrons in Fig. 10a and thermal neutrons in Fig. 10b. Again, we do not display the fast pdfs of assembly 2 as the average number of particles is so low due to either down-scatter to the thermal range or leakage from the system and the relative standard deviation is much larger than the average. As expected, the pdfs of the more severe reactivity insertions have much larger population averages. This can be explained by considering the extreme case of $t_{in} = 0.01\tau_2^1(0)$ (the blue and red lines), where the system is only briefly subcritical and is highly supercritical for $\sim 99\%$ of the simulation- it is also for this reason that the statistics

are not as well converged as the other distributions because of the larger number of divergent chains (which corresponds to sampled $\Delta t \to 0$). We are able to discern that the fast distributions are still atop the gamma fit (more so than on the Gaussian) while the thermal distributions for the longer times appear to agree with the gamma fits as well. This suggests that once a distribution's standard deviation relative to the mean has decreased enough, it will agree more closely with a gamma distribution, even when the fitted gamma distribution has not converged to its asymptotic Gaussian shape.

7. Conclusions

The central goal of this investigation was to establish the validity of the two-parameter gamma distribution in describing the neutron number pdf for both isolated and coupled multiplying assemblies containing spontaneous fission sources. Following a conjecture due to Harris, the two parameters were fixed by enforcing preservation of the first and second moments (the mean and the variance) of the true distribution. The exact fast and thermal energy group moment equations, obtained from a forward Master equation formulation, were numerically solved for two assemblies with both static and dynamic reactivity insertion. Assembly coupling coefficients were obtained from a previously published view factor method. In each case, the gamma distribution for the individual assemblies was compared with simulation results from a special purpose kinetic Monte Carlo code based on Gillespie's Stochastic Simulation Algorithm (SSA).

In the case of isolated one-group supercritical assemblies, the gamma distribution becomes an excellent approximation at $t > 20\tau$ and $n > 10$, for which the relative error is on the order of 1% within statistical noise for the tail of the distribution. On the other hand, isolated subcritical systems never approach a gamma-like distribution, with the relative error well-above 10% for the entire number distribution. For a supercritical assembly interacting with a subcritical assembly, even with relatively weak coupling the neutron number in the latter assembly rapidly becomes tied to that in the former assembly and the gamma distribution again becomes an accurate approximation in less than 100 lifetimes. Similar rapid relaxation to a gamma distribution was observed for two energy groups in the coupled case (within 5 thermal neutron lifetimes), with the primary difference that the fast neutron distribution shape is monotonically decreasing while the thermal neutron distribution evolves into a unimodal distribution. This behavior is consistent with the magnitude of the shape parameter η in the gamma distribution, i.e., $\eta < 1$ in the fast group, corresponding to a weak neutron source due to spontaneous fission and fast neutron leakage from the second assembly, and $\eta > 1$ in the thermal group, corresponding to a strong neutron source due to downscatter and both thermal and fast neutron leakage from the second assembly. Finally, for several time-dependent reactivity insertions of differing severity, the same behavior was observed for the number distributions.

Although computational demands of the Monte Carlo simulation made it difficult to carry out detailed quantitative error comparison across the entire distribution, our results do lend credibility to Harris' ansatz in that the gamma distribution normalized to the true mean and variance accurately reproduces the neutron number distribution, certainly over the bulk of the distribution and when population extinction is an extremely unlikely occurrence. It would be interesting and obviously very useful to carry out a similarly detailed comparative exercise for unlumped geometries, to see if finite size, neutron phase space dependence, and heterogeneities in the medium properties weaken the Harris ansatz. The moment equations, being linear adjoint transport equations, can be readily solved numerically to completely characterize the gamma distribution in this case. However obtaining accurate benchmark quality Monte Carlo results for the number distribution to assess the accuracy of the gamma distribution will be a challenge.

Acknowledgements

This work was supported by the US Department of Energy through the Los Alamos National Laboratory. Los Alamos National Laboratory is operated by Triad National Security, LLC, for the National Nuclear Security Administration of U.S. Department of Energy (Contract No. 89233218CNA000001). The authors gratefully acknowledge helpful discussions with Erin Davis and Scott Ramsey.

References

[1] BELL, G.I., "Probability Distribution of Neutrons and Precursors in a Multiplying Assembly," *Annals of Physics*, **21**, 243-283 (1963).

[2] BELL, G., "On the Stochastic Theory of Neutron Transport," *Nuclear Science and Engineering*, **21**, 390-401 (1965).

[3] PÁZSIT, I. and PÁL, L., *Neutron Fluctuations*, Elsevier, Oxford, UK (2008).

[4] BELL, G., and LEE, C., " On the Probability of Initiating a Persistent Fission Chain," LA-2608, Los Alamos National Laboratory, 1976.

[5] BAKER, R., "Deterministic Methods for Time-Dependent Stochastic Neutron Transport," *International Conference on Mathematics and Computational Methods Applied to Nuclear Science & Engineering*, 2009.

[6] O'ROURKE, P.F. and PRINJA, A.K., "Solution of the Neutron Survival Probability Equation Using k-Eigenmode Expansion," *Annals of Nuclear Energy*, **134**, 178-192, 2019.

[7] HANSEN, G.E., "Assembly of Fissionable Material in the Presence of a Weak Neutron Source," *Nuclear Science and Engineering*, **8**, 709-719 (1960).

[8] PRINJA, A., and SOUTO, F., "Probability Distributions for Neutron Multiplying Systems without Delayed Neutrons," Los Alamos National Laboratory report LA-UR 09-07886 (2009).

[9] HARRIS, D.R., *Naval Reactors Handbook*, Vol. 1, "Selected Basic Techniques," Chapter 5 (1964).

[10] AUTHIER, N., RICHARD, B., and HUMBERT, P., "Initiation of Persistent Fission Chains in the Fast Burst Reactor Caliban," *Nuclear Science and Engineering*, **177**(2), 169-183 (2014).

[11] WILLIAMS, M.M.R., "Burst Wait-Times in the Caliban Reactor Using the Gamma Probability Distribution Function," *Nuclear Science and Engineering*, **183**(1), 116-125 (2016).

[12] DAVIS, E.J. and PRINJA, A.K., "A Deterministic Transport Method for Calculating the Moments of the Fission Number Distribution," USB Proceedings, *International Conference on Mathematics & Computational Methods Applied to Nuclear Science & Engineering*, Jeju, Korea, April 16-20, 2017.

[13] GILLESPIE, D.T., "A General Method for Numerically Simulating the Stochastic Time Evolution of Coupled Chemical Reactions," *J. Comput. Phys.*, **22**(4), 403-434 (1976).

[14] O'ROURKE, P.F. and PRINJA, A.K., "Methods for Calculating Neutron Transfer Probabilities Between Assemblies," *Nuclear Science and Engineering*, (2022). DOI: 10.1080/00295639.2022.2106728

[15] PRINJA, A., and SOUTO, F., "Some Considerations on Stochastic Neutron Populations," *Trans. Am. Nucl. Soc.*, **102**, 255-257 (2010).

[16] FICHTL, E. and BAKER, R., "Computing the Moments of the Neutron Population Using Deterministic Neutron Transport." *International Conference on Mathematics and Computational Methods Applied to Nuclear Science & Engineering* Sun Valley, Idaho, May 5-9, 2013.

[17] BARTLETT, M.S., "Stochastic Processes or the Statistics of Change," *J. R. Stat. Soc. C*, **2**(1), 44-64, 1953. DOI:10.2307/2985327.

[18] FICHTHORN, K.A. and WEINBERG, W.H., "Theoretical Foundations of Dynamical Monte Carlo Simulations," *J. Chem. Phys.*, **95**(2), 1090-1096, 1991.

[19] MATTHES, W., "Statistical Fluctuations and Their Correlation in Reactor Neutron Distributions," *Nukleonik*, **4**, 213 (1962).

[20] DALFES, A., "Functional Analysis of the Random Processes in Nuclear Reactors," *Nukleonik*, **8**, 123 (1967).

[21] MATTHES, W., "Theory of Fluctuations in Neutron Fields," *Nukleonik*, **8**, 87 (1966).

[22] STACEY Jr., W.M., "Stochastic Kinetic Theory for a Space- and Energy-Dependent Zero-Power Nuclear Reactor Model," *Nucl. Sci. Eng.*, **36**, 389 (1969).

[23] GANG, X., "The Simulation of Probability Distribution of the Burst Waiting Time of Neutron Initiation," *Nucl. Sci. and Eng.*, **169**, 56 - 67, 2011.

[24] SUTTON, T.M., LaCHARITE, A.D., PRINJA, A.K. "Marduk: A Monte Carlo Code for Analyzing Stochastic Neutron Population Dynamics," *International Conference on Mathematics & Computational Methods Applied to Nuclear Science & Engineeering*, 2017.

[25] LEWIS, E. E., and MILLER, W. F., *Computational Methods of Neutron Transport*, New York: Wiley, 1984.

[26] SPRIGGS, G.D., BUSCH, R.D., "On the Definition of Neutron Lifetimes in Multiplying and Non-multiplying Systems," Los Alamos National Laboratory report LA-13260-MS, 1997.

[27] SHAMPINE, L.F., and GORDON, M.K., *Computer Solution of Ordinary Differential Equations: The Initial Value Problem* Freeman, San Francisco, 1975.

[28] O'ROURKE, P., "Modeling and Simulation of Stochastic Neutron and Cumulative Deposited Fission Energy Distributions." PhD Dissertation. University of New Mexico, 2020.

[29] LEEMIS, L.M. and MCQUESTION, J.T., "Univariate Distribution Relationships," *American Statistician*, **62**(1), 45-53, 2008.

Table 8: Coefficients of polynomial fits (see Eq. 43)

(a) For $t_{in} = 0.01\tau_2^1(0)$

	c_4	c_3	c_2	c_1	c_0
$k_{\text{eff},1}$	0	$5.60968 \cdot 10^{11}$	$-1.34235 \cdot 10^{7}$	$3,836.37$	0.498436
ϱ	$1.73644 \cdot 10^{17}$	$-1.47160 \cdot 10^{13}$	$1.10706 \cdot 10^{9}$	$5.27407 \cdot 10^{4}$	9.02805
$\lambda_{f,1}^1$	$4.14887 \cdot 10^{19}$	$-4.04047 \cdot 10^{15}$	$2.24620 \cdot 10^{11}$	$2.65780 \cdot 10^{6}$	374.621
$\lambda_{f,2}^1$	$2.24811 \cdot 10^{19}$	$-2.18978 \cdot 10^{15}$	$1.21667 \cdot 10^{11}$	$1.42945 \cdot 10^{6}$	200.835
$\lambda_{c,1}^1$	$1.79797 \cdot 10^{16}$	$-1.75100 \cdot 10^{12}$	$9.73429 \cdot 10^{7}$	$1,151.80$	0.162347
$\lambda_{c,2}^1$	$3.79270 \cdot 10^{18}$	$-3.69430 \cdot 10^{14}$	$2.05260 \cdot 10^{10}$	$2.41157 \cdot 10^{5}$	33.8821
$\lambda_{\ell,1}^1$	$1.54619 \cdot 10^{19}$	$-4.52878 \cdot 10^{14}$	$1.63787 \cdot 10^{11}$	$2.09524 \cdot 10^{7}$	$3,717.77$
$\lambda_{\ell,2}^1$	$1.23407 \cdot 10^{16}$	$-4.65227 \cdot 10^{11}$	$1.46661 \cdot 10^{4}$	$1.22141 \cdot 10^{8}$	2.73307
$\lambda_{s,1\to2}^1$	$2.62997 \cdot 10^{19}$	$-2.56126 \cdot 10^{15}$	$1.42387 \cdot 10^{11}$	$1.68478 \cdot 10^{6}$	237.472

(b) For $t_{in} = 0.1\tau_2^1(0)$

	c_4	c_3	c_2	c_1	c_0
$k_{\text{eff},1}$	0	$5.60968 \cdot 10^{8}$	$-1.34235 \cdot 10^{5}$	383.637	0.498436
ϱ	$1.736444 \cdot 10^{13}$	$-1.47160 \cdot 10^{10}$	$1.10706 \cdot 10^{7}$	$5,274.07$	9.02805
$\lambda_{f,1}^1$	$4.14887 \cdot 10^{15}$	$-4.04047 \cdot 10^{12}$	$2.24620 \cdot 10^{9}$	$2.65780 \cdot 10^{5}$	374.6218
$\lambda_{f,2}^1$	$2.24811 \cdot 10^{15}$	$-2.18978 \cdot 10^{12}$	$1.21667 \cdot 10^{9}$	$1.42945 \cdot 10^{5}$	200.835
$\lambda_{c,1}^1$	$1.79797 \cdot 10^{12}$	$-1.75100 \cdot 10^{9}$	$9.73429 \cdot 10^{5}$	115.180	0.162347
$\lambda_{c,2}^1$	$3.7927 \cdot 10^{14}$	$-3.69430 \cdot 10^{11}$	$2.05260 \cdot 10^{8}$	$2.41157 \cdot 10^{4}$	33.8821
$\lambda_{\ell,1}^1$	$1.54619 \cdot 10^{15}$	$-4.52878 \cdot 10^{11}$	$1.63787 \cdot 10^{9}$	$2.09524 \cdot 10^{6}$	$3,717.77$
$\lambda_{\ell,2}^1$	$1.23407 \cdot 10^{12}$	$-4.65227 \cdot 10^{8}$	$1.22141 \cdot 10^{6}$	$1,466.61$	2.73307
$\lambda_{s,1\to2}^1$	$2.62997 \cdot 10^{15}$	$-2.56126 \cdot 10^{12}$	$1.42387 \cdot 10^{9}$	$1.68478 \cdot 10^{5}$	237.472

(c) For $t_{in} = 0.5\tau_2^1(0)$

	c_4	c_3	c_2	c_1	c_0
$k_{\text{eff},1}$	0	$4.48774 \cdot 10^{6}$	$-5,369.43$	76.7274	0.498436
ϱ	$2.77831 \cdot 10^{10}$	$-1.17728 \cdot 10^{8}$	$4.42826 \cdot 10^{5}$	$1,054.81$	9.02805
$\lambda_{f,1}^1$	$6.63819 \cdot 10^{12}$	$-3.23238 \cdot 10^{10}$	$8.98483 \cdot 10^{7}$	53156.0	374.621
$\lambda_{f,2}^1$	$3.59697 \cdot 10^{12}$	$-1.75182 \cdot 10^{10}$	$4.86670 \cdot 10^{7}$	$28,589.0$	200.835
$\lambda_{c,1}^1$	$2.87676 \cdot 10^{9}$	$-1.40080 \cdot 10^{7}$	$38,937.2$	23.0360	0.162348
$\lambda_{c,2}^1$	$6.06832 \cdot 10^{11}$	$-2.95544 \cdot 10^{9}$	$8.21042 \cdot 10^{6}$	$4,823.15$	33.8821
$\lambda_{\ell,1}^1$	$2.47391 \cdot 10^{12}$	$-3.62303 \cdot 10^{9}$	$6.55149 \cdot 10^{7}$	$4.19049 \cdot 10^{5}$	$3,717.77$
$\lambda_{\ell,2}^1$	$1.97452 \cdot 10^{9}$	$-3.72182 \cdot 10^{6}$	$48,856.6$	293.322	2.73307
$\lambda_{s,1\to2}^1$	$4.20796 \cdot 10^{12}$	$-2.04901 \cdot 10^{10}$	$5.69550 \cdot 10^{7}$	$33,695.7$	237.472

Highlights:

- Derive forward master equation and moment equations for two coupled reactors with fast and thermal neutrons.
- Apply the stochastic simulation algorithm to solve the forward master equation via Monte Carlo sampling
- Test the validity of the Harris ansatz for two coupled reactors with fast and thermal neutrons with time-dependent reactivity insertion.

CRediT:

Patrick O'Rourke: Software, Validation, Formal analysis, Investigation, Writing - original draft

Anil Prinja: Conceptualization, Methodology, Resources, Validation, Writing - review & editing, Supervision, Project administration, Funding acquisition

Declaration of interests

☒ The authors declare that they have no known competing financial interests or personal relationships that could have appeared to influence the work reported in this paper.

☐The authors declare the following financial interests/personal relationships which may be considered as potential competing interests: